Turk J Pharm Sci 2026;23(2):85-104
DOI: 10.4274/tjps.galenos.2026.10001

ORIGINAL ARTICLE

Development of Mucoadhesive Nanofiber as an Alternate Therapeutic Regimen for Subclinical Endometritis in Cattle

Priyanka KUMARI[1], Shivlal YADAV[1], Ashutosh TRIPATHI[2], Manish Kumar SHUKLA[3], Surabhi PARANGI[4], Janmejay PANDEY[4], Rakesh Kumar SAHOO[5], Goutam RATH[5], Debasmita DUBEY[6], Amit Kumar GOYAL[1]*

[1]Central University of Rajasthan, Department of Pharmacy, Ajmer, Rajasthan, India
[2]Sardar Vallabhbhai Patel University of Agriculture and Technology, College of Veterinary and Animal Sciences, Department of Livestock Farm Complex, Meerut, Uttar Pradesh, India
[3]Sardar Vallabhbhai Patel University of Agriculture and Technology, College of Veterinary and Animal Sciences, Department of Veterinary Gynaecology and Obstetrics, Meerut, Uttar Pradesh, India
[4]Central University of Rajasthan, Department of Biotechnology, Ajmer, Rajasthan, India
[5]Siksha 'O' Anusandhan School of Pharmaceutical Sciences, Bhubaneswar, Odisha, India
[6]Siksha 'O' Anusandhan, IMS and Sum Hospital, Department of Medical Research, Bhubaneswar, Odisha, India

ABSTRACT

Objectives: Subclinical endometritis in cattle is still a problem that has a detrimental effect on dairy production and fertility. Traditional intrauterine or systemic antibiotic treatments frequently result in suboptimal uterine drug levels, encourage resistance, and increase the possibility of drug residues in food items. The current study aimed to treat subclinical endometritis in repeat breeders by creating and testing an ofloxacin (Ofx)-loaded mucoadhesive polyvinyl alcohol/chitosan nanofiber using the electrospinning technique.

Materials and Methods: The process constants were optimised using a central composite design to create a uniform nanofiber with maximum mechanical properties. Furthermore, *in vitro* (drug release, antibacterial activity), *ex vivo* (mucoadhesion and retention), and *in vivo* (endometrial cytology and plasma drug concentration) parameters were evaluated.

Results: The scanning electron microscopy image of Ofx nanofiber suggests a diameter of 190–210 nm and tensile strength of 1.33 tensile strength with an entrapment efficiency of 97.54 ± 0.89%. Ofx delivered via nanofiber exhibited sustained release of Ofx up to 216 hours. *Ex vivo* assessments demonstrated stronger adherence and higher retention, while *in vitro* studies showed no cytotoxic effects. *In vivo* studies on the cattle suggested suitability for localized intrauterine administration. These findings indicate that encapsulation of Ofx in nanofibers stabilises the formulation and offers enhanced treatment efficiency compared to a conventional treatment regimen for subclinical endometritis in repeated breeders.

Conclusion: Ofx-loaded nanofibers offer a novel and promising localized and mucoadhesive drug delivery approach for subclinical endometritis in cattle. Future research must prioritise further *in vivo* validation, long-term reproductive effects, and resistance management to translate into practical veterinary uses.

Keywords: Ofloxacin, nanofiber, mucoadhesive, QbD, CCD, subclinical endometritis, chitosan, PVA, pharmacokinetic parameters

***Correspondence:** amitkumargoyal1979@gmail.com, **ORCID-ID:** orcid.org/0000-0002-6045-3525

Received: 06.10.2025 **Accepted:** 18.08.2026 **Publication Date:** 01.09.2026

Cite this article as: Kumari P, Yadav S, Tripathi A, Shukla M, Surabhi S, Pandey J, Sahoo RK, Rath G, Dubey D, Goyal AK. Development of mucoadhesive nanofiber as an alternate therapeutic regimen for subclinical endometritis in cattle. Turk J Pharm Sci. 2026;23(2):85-104

INTRODUCTION

Dairy animals can suffer from subclinical endometritis (SE), a uterine condition that affects reproduction without obvious clinical signs, affecting about 30% globally.[1] Unlike clinical endometritis, SE is characterized by endometrial inflammation that is only detectable through cytological or histological testing. Often overlooked by farmers and veterinarians, SE negatively impacts conception rates, prolongs the interval between calving and conception, and increases culling, leading to significant financial losses in the dairy industry.[2] Its pathophysiology is linked to abnormal postpartum inflammatory responses, persistent bacterial infections, poor uterine involution, and immunological dysregulation.[3]

Numerous investigations argue that *Fusobacterium necrophorum, Escherichia coli, Trueperella pyogenes, Prevotella* spp., and *Staphylococcus* spp. (including coagulase-negative strains and *S. aureus*), are the prominent uterine pathogens that play a significant role in the pathophysiology of SE.[4] These pathogens become problematic at post-parturition due to factors like delayed placenta and messy calving techniques, resulting in infertility, inflammation, and disruptions in the oestrous cycle.[5,6] The diagnosis of SEs remains challenging as it is often asymptomatic; however, methods such as low-volume uterine lavage or cytobrush for measuring polymorphonuclear neutrophils are used for assessment.[7]

Therapy using hormones, antiseptic sanitation, and antibiotics has historically been employed to treat bacterial infections; however, their application in specific environments has resulted in prolonged interventions and the emergence of multidrug-resistant bacterial strains.[8,9] These treatment protocols frequently fail to achieve adequate drug concentrations in uterine tissue, leading to systemic toxicity and antibiotic resistance, alongside potential residues in milk and meat.[10] Intrauterine treatments suffer from reduced drug retention due to contractions and discharge, complicating the evaluation of treatment impacts on reproductive success without clear diagnostic criteria.[11] The public health concern regarding antibiotic resistance and residues in food animals underscores the shortcomings of conventional systemic treatments for uterine infections, which often show ineffectiveness, adverse effects, and insufficient tissue penetration.[12] This highlights the urgent need for localized treatment approaches, such as mucoadhesive drug delivery systems (MDDS), which are designed to adhere to mucosal tissues, facilitating prolonged drug residence at infection sites while minimizing systemic effects.[13,14] MDDSs enhance therapeutic efficacy and lower the risk of antimicrobial resistance, systemic toxicity, and drug overuse, improving treatment compliance and reducing economic burdens through controlled and sustained drug release.[15,16]

Nanofibers (NFs) are emerging as effective frameworks for MDDS, facilitating the targeted delivery of therapeutic agents across mucosal tissues.[17] This approach minimizes drug dosage, reduces wastage, and diminishes the risk of systemic side effects and drug resistance.[18] A key method for producing these polymeric NFs is electrospinning, which involves applying an electric field to a polymeric solution, resulting in the formation of thin fiber membranes on a collector.[19] Various factors, including the strength of the electric field, the distance between the nozzle and the collector, environmental conditions, and the properties of the polymer solution, influence the quality of NF production.[20,21]

Commonly used polymers for developing mucoadhesive NFs include chitosan (CS) and polyvinyl alcohol (PVA).[22] Both are biocompatible and non-toxic, with PVA providing advantageous traits such as water solubility and mechanical stability, while CS offers biodegradability and antibacterial properties.[23] CS's ability to dissolve in acidic conditions makes it suitable for targeting drug release at diseased tissues.[24] The combination of PVA and CS results in hybrid NFs that enhance drug retention and stability on mucosal surfaces while promoting controlled release through pH-responsive mechanisms.[25] Therefore, PVA/CS electrospun NFs are posited as a versatile and cost-effective solution for prolonged, localized drug administration in biomedical contexts.[26]

Ofloxacin (Ofx), a fluoroquinolone antibiotic, is noted for its effectiveness against a wide range of bacterial organisms and is considered a potential treatment for endometritis.[27,28] It acts by inhibiting crucial bacterial enzymes necessary for DNA replication, offering a dual-target approach that enhances efficacy while minimizing the development of resistance.[29] With favourable pharmacokinetic properties, including significant tissue penetrability and prolonged activity, Ofx is an ideal candidate for localized application within the uterine environment.[30,31]

The goal of the currently designed study was to treat SE in repeat breeders by developing and conducting tests on an Ofx-loaded mucoadhesive PVA/CS NF via the electrospinning approach. The process parameters were optimized using a central composite design (CCD) to produce a uniform NF with enhanced loading capacity. Additionally, *ex vivo* (mucoadhesion and retention), *in vitro* (drug release and antibacterial activity), and *in vivo* (endometrial cytology) parameters were evaluated. This study addresses the drawbacks of traditional treatment techniques and proposes a new, efficient, and focused strategy for controlling SE.

MATERIALS AND METHODS

Ofx was snapped up from Sigma Aldrich. CS (Deacetylated ± 75%, Shrimp shell), PVA (M.W. 60-1.25 KDa), Acetic acid acquired from Himedia. Other chemicals used in the experiments were of analytical grade. Acetonitrile and methanol [high-performance liquid chromatography (HPLC) grade] were purchased from Thermo Fisher Scientific (U.K.).

PVA/CS NF formulation development and optimization

PVA solution (10% w/v) was prepared in 10 mL of hot distilled water (< 60 ºC). Then, 2% (w/v) CS was initially soaked by adding 0.2 g in 10 mL of aqueous acetic acid solution (2% v/v) overnight. CS and PVA solutions were stirred separately until a clear solution was obtained. Furthermore, solutions of PVA

and CS were combined in ratios of 9:1, 8:2, and 7:3 and stirred for 6 hours at room temperature (RT) to obtain a clear and homogeneous solution.

The devised blend was electrospun through E-Spin Nanotech (Central University of Rajasthan). The above-prepared PVA/CS solution was loaded and pumped out through a 5 mL syringe, keeping the tip-to-collector distance at 12 cm, and electrospinning was carried out under ambient conditions (temperature: 32 ± 2 °C; relative humidity: 33-50%). The applied high voltages ranged from 18 to 21 kV, with the flow rate (0.5 to 1.5 µL/hr) as the independent variable. This relatively low flow rate was optimized to ensure stable Taylor cone formation, minimize bead formation, and produce uniform NFs by allowing sufficient time for solvent evaporation during jet travel, particularly given the polymeric system's viscosity and intermolecular interactions. All the electrospun NFs were collected on aluminum foil and then placed in a desiccator for 1 day at RT to cross-link in glutaraldehyde vapor (15 mL of 50% v/v). After cross-linking, the fibers were kept in the desiccator for an additional 24 hours to facilitate the removal of excess glutaraldehyde vapor.[32]

The first step in developing a formulation is to optimize the formulation with the variables, which may be accomplished using software or a one-factor-at-a-time experiment. In this experimental design, a CCD was employed to optimize the PVA/CS NFs using Design-Expert (version 13.0.5.0, Stat–Ease, Minneapolis, MN).[33] The ratio of CS used in PVA/CS, the voltage applied to stretch the polymer from tip to collector to form a thread-like structure, and the flow rate of polymer oozing from the needle were taken as independent variables. The impact of these independent factors on fiber diameter and tensile strength (MPa) was optimized by response surface methodology. Seventeen experiments were conducted to run CCD and to analyze optimal responses for NF diameter and MPa, as shown in Table 1. It reduces the duration of experiments and unnecessary expenses. It helps create response surface plots that reveal interaction effects and highlight the optimal conditions for achieving the desired NF characteristics. CCD also generated a non-linear second-order quadratic equation, as illustrated in the equation.

$$Y = \beta_0 + \beta_1 A + \beta_2 B + \beta_3 C + \beta_3 C + \beta_{12} AB + \beta_{13} AC + \beta_{23} BC + \beta_{11} A^2 + \beta_{22} B^2 + \beta_{33} C^2 \quad \text{(i)}$$

A, B, C = independent factor, β_0 = intercept, β_1, β_2, β_3 = regression coefficients, β_{12}, β_{13}, β_{23} = regression coefficients interaction, β_{11}, β_{22}, β_{33} = quadratic terms, respectively.[34]

The statistical significance of the model was assessed using analysis of variance (ANOVA), as indicated by the *p*-value, determination coefficient, correlation coefficients, adjusted R^2, sufficient precision, and coefficient of variance for each response.[35]

Table 1. The experimental design's variables of intervention, the corresponding respondent variables, and desirability.[36]

Independent factors (X)	Unit	Level		
		-1	0	+1
Cs	Ratio	1	2	3
Voltage	kV	18	19.5	21
Feed rate	µl/hr	0.5	1	1.5
Dependent factors (Y)	**Unit**	**Response with desirability**		
Fiber diameter	nm	Minimum		
Tensile strength	MPa	Maximum		

Characterization

Scanning electron microscopy (SEM)

Using SEM, the NF's structural traits were evaluated (Thermo Fisher Scientific, Central University of Rajasthan). A 1 × 1 cm^2 NF was coated with gold, sputtered, and imaged at 20 kV. Fifty arbitrarily chosen fibers were used to calculate the mean diameter of the fiber using ImageJ software, and a frequency size distribution curve was plotted in Origin software.

Swelling index

To calculate the swelling index of the produced NFs, the specimen was weighed initially in a dried condition and then stored at 37 ± 1°C in an agar gel plate with 15 mL of 2% w/v agar. After a different time interval, the NFs were weighed again. The following formula was used to determine the swelling index:

$$\%\ Swelling\ Index = \frac{final\ weigth\ (t) - Initial\ weigth}{Initial\ weight} * 100 \quad \text{(ii)}[37]$$

MPa

The Instron-5967 testing equipment measured the MPa of blank NFs (B-NF) and Ofx-NFs. The NFs were fragmented into a rectangular form (5 × 30 mm^2) and secured in an Instron Jaws Tensile-clamped paper holder. At RT, the 50 N tension was torqued at an expansion rate of 5 mm/min.[38]

Fourier-transform infrared spectroscopy (FTIR)

The chemical structure and alteration were identified by FTIR (PerkinElmer spectrometer, Central University of Rajasthan). The sample was mixed with FTIR-grade KBr in a 1:100 ratio to prepare thin pellets for analysis. Spectra of the drug, excipient, and formulation were taken in the 4000–400 cm^{-1} range and plotted in Origin.

Differential scanning colorimeter (DSC)

DSC (Netzsch Geratebau GmbH, Germany) experiments were performed on pure Ofx, CS, PVA, B-NF, and Ofx-NF. An appropriate quantity of sample was taken, sealed in an aluminum pan, and heated at 10 °C/min under a nitrogen atmosphere. Thermograms of the samples were observed at a range between 0 °C to 300 °C.[39]

Drug loading and encapsulation

An Agilent Cary 60 UV-Vis spectrophotometer was used to measure the drug loading and the quantity of Ofx trapped in the designed nanofibrous mat. 2 x 2 cm^2 of the optimized nanofibrous matrix was weighed and submerged in 10 milliliters of simulated uterine fluid (SUF) (pH~6.8) using a sonicator and mechanical shaking. Before analysis, the solution was centrifuged and filtered through a 0.45 μm filter. The concentration of Ofx was analyzed at 287.5 nm. The calibration curve was produced in SUF (pH~6.8) (composition mentioned in Table 2).[40] The formula for calculating the mass of Ofx retrieved (W_{uv}) was calculated as concentration × total volume. The total drug distribution during fabrication of the NF mat was 20 mg in a 320 cm^2 nanofibrous mat; the theoretical drug content in a 2 × 2 cm^2 sample calculated was approximately 0.25 mg.

Table 2. Composition of simulated uterine fluid (pH 6.8).

Chemical name	Quantity (g/L)
NaCl	4.97
KCl	0.224
$CaCl_2$	0.167
$NaHCO_3$	0.25
Glucose	0.5
$NaH_2PO_4{\cdot}2H_2O$	0.072

NaCl, sodium chloride; KCl, potassium chloride, $CaCl_2$, calcium chloride; $NaHCO_3$, sodium bicarbonate; $NaH_2PO_4{\cdot}2H_2O$, sodium dihydrogen phosphate dihydrate.

$$\%DL = \frac{Wuv}{Wnf} * 100 \quad \text{(iii)}$$

$$\%EE = \frac{Wuv}{Wes} * 100 \quad \text{(iv)}$$

Where W_{nf} is the weight of 2 x 2 cm^2 NF, Wes is the amount of Ofx added before the electrospinning process. The data were presented as mean ± standard deviation (SD), and all assays were made in triplicate (n = 3).

In vitro drug release and kinetics

The drug release profile of Ofx from NFs was evaluated using the dialysis method, which was filled with SUF. A 2 x 2 cm^2 Ofx-NF was added to a 5 cm dialysis membrane-50 (MWCO: 12–14 kDa) and immersed in 50 mL SUF at 37 °C. The medium was continuously stirred at 100 rpm to ensure proper mixing of diffused Ofx from the membrane. At a predetermined time, 5 mL of the sample was collected and returned with fresh medium. The samples were further analyzed using a UV-Vis spectrophotometer at 287.5 nm. A standard calibration curve (R^2 = 0.9988) was prepared to determine the drug concentration. The DD Solver add-in software was used to construct and monitor various kinetic models and to investigate the improved drug release kinetics of Ofx from NFs.[41]

Ex vivo permeation of Ofx

The Franz diffusion cell was used for the permeation study on the uterine mucosa. The goat's uterine mucosa was obtained from a nearby slaughterhouse, cleaned with 0.9% w/v saline solution, and preserved in formalin before the experiment. The mucosa was positioned between the donor and receptor compartments of a 25 mL Franz diffusion cell, which was the recommended model. The two compartments of the Franz cell were then secured together after a strip of the NF film was placed on the mucosa. Throughout the investigation, the shaker was operated at 100 rpm, and the temperature was maintained at 37 ± 1 °C. For up to 8 hours into the trial, samples were collected via lumbar puncture at predetermined intervals. To maintain a consistent volume, 1 mL samples were collected at each interval and replaced with the same volume of new medium. All *ex vivo* permeation studies were performed in triplicate under identical experimental conditions to ensure reproducibility. A UV spectrophotometer was used to determine the amount of Ofx in the filtered samples. A graph of cumulative Ofx penetrated through the mucosa (μg/cm^2) against time (min) was also used to determine the permeability of Ofx from the NF film. The slope of the graph was used to calculate the permeability flow using linear regression. The apparent permeation coefficient was determined.

$$Papp = \frac{dQ}{dt}/(A.Co) \quad \text{(vi)}$$

dQ/dt = rate of drug transport across the membrane (μg/s)

A = surface area of the membrane (1 cm^2)

Co = initial drug concentration in the donor (μg/mL).

Plotting the amount of Ofx penetrated against time yielded a graph, the slope of which indicated the steady-state flow value (J = μ/cm^2/h). However, there is a metric that may be applied to determine flow.

$$J = \frac{dQ}{dt} * A \quad \text{(vii)}[42]$$

Mucoadhesion test

Fresh goat uterine mucosa and a modified manual glass-slide technique, adapted from popular *ex vivo* adhesion tests, were used to assess mucoadhesion.[43] The mucosal side of fresh mucosa was cleansed, clipped, and used within two hours of collection. It was adhered to a stiff glass slide. A second glass slide was brought into contact with a NF patch measuring about 1 × 1 cm^2, which was applied to the mucosa. A 50-g preload weight was applied for 60 seconds to ensure close contact. Following the contact period, tiny calibrated weights were added to the upper slide, one at a time, until detachment occurred; the total mass at detachment was recorded. The formula for detachment force (N) was mass (kg) × 9.81 ($m{\cdot}s^{-2}$). Six sextuplicate tests were conducted for

each formulation. The mucosa sample assembly was placed on a slanted holder, and SUF (0.5 mL·min^{-1}) was flowed down the outermost layer to assess the residence duration under steady PBS flow at 37 °C. The time until complete expulsion of NFs was noted.

Cell viability assay

A colourimetric MTT experiment was used to assess the cell viability of the proposed NF-based formulations, i.e., B-NF and Ofx-NF, compared to pure Ofx, following an approved protocol.[44] This MTT-mediated cell toxicity investigation was conducted on HeLa cells. To provide consistent conditions in each well, adherent cells were concentrated in 96-well plates (TPP96, Hi Media Laboratories) at a density of 10^4 cells per well. The cells sown in the plates were cultured for 24 hours in a CO_2 incubator (Heracell 150i, ThermoFisher). To investigate the effect of Ofx and nanoformulation, various concentrations of each material have been produced using culture media. The maximal drug concentration for HeLa cells was 100 μM. The HeLa cells on the culture plates were incubated for twenty-four hours after receiving the therapy with the indicated concentrations of pure Ofx, B-NF, and Ofx-NF. Throughout the entire experiment, culture media were regarded as the control. After the incubation period, 50 μL of 3-(4,5-dimethylthiazol-2-yl)-2,5-diphenyltetrazolium bromide (MTT) solution (5 mg/mL) was applied to each well of the 96-well plate. Dimethyl sulfoxide (150 μL) was added to MTT-treated plates after incubating them for an additional four hours. This caused the formazan crystals to disintegrate and turn a purplish colour. The absorbance of each specimen at λmax 570 nm was measured using a microplate reader. The IC_{50} value and percentage viability graph were plotted against the concentration of pure Ofx, B-NF, and Ofx-NFs in relation to HeLa cells. All experiments were performed in triplicate, and the results are expressed as mean ± SD. Statistical analysis was performed using two-way ANOVA.

Antimicrobial activity

The antibacterial properties of B-NFs and Ofx-NFs were evaluated using the agar disc diffusion technique against the bacterial strains *S. aureus* and *E. coli* (both gram-negative and gram-positive). The agar plate was prepared by pouring 30 mL of nutrient agar into petri plates, and then 100 μL of bacterial suspension was evenly distributed on the plates. Then, the plate was allowed to add B-NFs and Ofx-NFs and be maintained at 37 °C in an incubator for 24 hr. The experiment was carried out three times to observe the inhibitory zone.[45]

In vivo study

All animal experiments adhered to the CPCSEA guidelines and received approval from the IAEC of Sardar Vallabh Bhai Patel University (approval no: IAEC/SVPUAT/2022/109, dated May 24, 2022).

This study did not involve human participants; hence, patient consent was not required.

A total of 24 indigenous cattle with SE, screened from the repeat breeder group, were enrolled for the study. The cattle were housed at LRC, SVPUAT, Meerut and nearby Gaushalas. The body condition score of the cattle under study was 3.5 or above and was maintained under optimum nutritional and management conditions.

The animals were randomly allocated into three groups (n = 8 per group) using a simple randomization approach to minimize selection bias. SE was diagnosed based on the presence of polymorphonuclear cells (PMNs) in the uterine cytology. The animals were randomly allocated into three groups (n = 8 per group) using a simple randomization approach to minimize selection bias. SE was diagnosed based on the presence of PMNs in the uterine cytology. Group I served as the untreated control. Group II (positive control) received Ofx (3 mg/kg), while Group III was administered Ofx-loaded NFs (Ofx-NF) intrauterinely (1 mg/kg). Treatments were administered for three consecutive days in Group II and as a single dose in Group III.

Due to practical constraints, blinding was not implemented during treatment administration; however, outcome assessment was performed by an independent investigator blinded to group allocation. All experimental procedures were conducted under standardized conditions to minimize bias. The sample size (n = 8 per group) was selected based on commonly reported group sizes in similar veterinary studies for comparative evaluation of treatment efficacy.

Endometrial samples for microbial culture were collected aseptically using a cytobrush following standard cytology protocols. Samples were collected twice from each animal: before treatment initiation (day 0) and 30–45 minutes prior to artificial insemination in the subsequent estrus cycle.

Isolation and identification of bacteria

The sample withdrawn for endometrial cytology was used for staining on brain heart infusion agar and MacConkey lactose agar plates, which were incubated at 37 °C for 24 hours in an aerobic incubator. To identify mould sp. and yeast sp., the Sabouraud dextrose agar plate was incubated at 37 °C and 25 °C, respectively. The bacteria were identified by their evolutionary history, chemical composition, colony morphology, and microscopic characteristics. Before molecular and resistance testing, the identified colonies were stored in glycerol stock at -20 °C. To subculture pure colonies for a further 24 hours, they were cultivated on blood agar at 37 °C.[46]

Vaginal mucus pH

Vaginal pH was measured once on day 0 and on the last day after the treatment.

Endometrial cytology

This method involved aseptically inserting the cytobrush (Marfair Surgical Corporation, Ludhiana) into the uterine canal after screwing it onto the cytobrush gun's piston. The cytobrush was softly brushed across the uterine endometrium and then drawn off in the cytobrush cannon. The brush was then pressed onto an uncontaminated glass microscopic slide, allowed to dry, and fixed with methanol, after which it was stained. The proportion of PMNs was determined by counting cells at 40X magnification (Olympus CX21, Japan). A valid diagnosis of SE required a threshold PMN volume of 5% or higher.[47]

Pharmacokinetic study

The *in vivo* pharmacokinetic study was conducted on the same experimental cattle mentioned. The calves were treated with the tailored pure Ofx, Ofx-NF, and Ofx-hydrogel formulations via the intrauterine route at a prescribed dosage for cattle. Ofx hydrogel was taken as an alternative novel drug delivery system, to be compared with the NF. The Ofx-loaded hydrogel (Ofx-hydrogel) was prepared as described previously,[31] with a composition consisting of PVA (10% w/v) and CS (2% w/v) in a ratio of (7:3). The blood samples (~5 mL) were drawn from the jugular vein into EDTA vials at prearranged intervals (0, 1, 2, 4, 6, 8, 10, 12, 16, 24, and 30 days). All samples were centrifuged at 3000 rpm for 10 minutes, and the plasma was stored at -20 °C until further analysis. The quantification of Ofx in plasma was performed using a validated reverse-phase high-performance liquid chromatographic method.[48] A standard stock solution (500 ppm) was generated by dispersing 0.5 mg of Ofx in 10 mL of a mobile phase containing 10 mM phosphate buffer (pH 3.0, modified with 10% o-phosphoric acid) and methanol (50:50 v/v). Working standards (2-10 μg/mL) were generated by successively diluting the stock solution, and blank bovine plasma was spiked with aliquots of these working standards to create calibration curves in the 0.05–10 μg/mL range. 200 μL plasma from each sample was processed by protein precipitation using three volumes of acetonitrile, vortexed, and centrifuged for 10 minutes at 10,000 rpm. The transparent supernatant was filtered using a 0.22 μm syringe filter before injection.[49] The NovaSil C18 100 Å column (250 × 4.6 mm, 5 μm) was used for chromatographic separation, with isocratic elution at a flow rate of 1.0 mL/min and detection at λ_{max} of 290 nm. The approach demonstrated good linearity with a correlation coefficient (R^2 = 0.998). The limit of detection (LOD) and limit of quantification (LOQ) were calculated using the equations LOD = 3.3σ/S and LOQ = 10σ/S. Non-compartmental analysis (PK Solver) was used to compute the pharmacokinetic parameters [C_{max} (maximum concentration), T_{max} (maximum time), area under the curve $(AUC)_{0-t}$, $AUC_{0-\infty}$, $t_{½}$ (half life), and mean residence time (MRT)].[50] The data were presented as mean ± SD, and two-way ANOVA was used to assess statistical significance ($p < 0.05$).

Pregnancy diagnosis

The pregnancy diagnosis was performed on day 45 following artificial insemination through rectal palpation and ultrasonography (Minitube, 6.5 MHz, rectal probe).[51]

Statistical analysis

Kinetic modeling was performed using the DD Solver add-in for Microsoft Excel, and non-compartmental pharmacokinetic parameters were analyzed using the PK Solver add-in for Microsoft Excel (written in Visual Basic for Applications). Statistical analysis of all experimental data was carried out using GraphPad Prism (version 8.0.1, Boston, USA).

All results are expressed as mean ± SD. Continuous variables, such as CFU count and PMN percentage, were analyzed using one-way ANOVA followed by Dunnett's multiple-comparison test. Categorical data, such as pregnancy rate, were analyzed using the chi-square test. Pharmacokinetic parameters were statistically compared using two-way ANOVA. A value of $p < 0.05$ was considered statistically significant.

RESULTS

Optimization of NF

PVA/CS NFs were prepared via electrospinning. The CS concentration in PVA/CS was a limiting factor in forming a spinnable solution. Changes in the electrospinning machine's flow rate and voltage significantly influence the formation of a continuous stretch jet to the collector, resulting in uniform NFs. Thus, optimized CS ratios were required to prepare PVA/CS NFs. The optimization of the formulation was carried out by the CCD using three independent variables: X1 = CS ratio in PVA/CS solution, X2 = applied voltage to form a jet of polymeric solution from the tip of the needle, and X3 = flow rate of the pump, which pushes the polymeric needle plunger to ooze out polymer. Seventeen runs were processed, and the design generated the levels (-1, 0, +1) and α (1.681). ANOVA was used to validate the effects of the independent variables (X1, X2, and X3) on the response variables [Y1 = NF diameter (nm) and Y2 = MPa], as listed in Table 3. These response variables were analyzed and fitted to various models, including linear, 2-factor interaction, quadratic, and cubic models. A suitable model was selected by determining the highest correlation coefficient value. Based on a significant *p*-value and sum of squares from a sequential model, the best fit model for each response was a quadratic model. Therefore, the quadratic model was used to elucidate the effects of the independent variables (CS ratio, voltage, and feed rate) on fiber diameter and MPa.[52]

Effect of input variables on NF diameter

The diameter of the B-NF was recorded in the range of 100–400 nm, based on the variation in the values of independent and dependent variables. The smallest diameter (173.14 nm) was observed for run 2, whereas the largest diameter (375.51 nm) was observed for run 17. The effect of variables on NF diameter suggests a quadratic model, which was effectively used to determine the correlation coefficient. Table 4 presents a summary of the statistical analysis of three independent variables on diameter, with R^2, adjusted R^2, and predicted R^2 of 0.9911, 0.9797, and 0.9389, respectively. Figure 1a represents the 3D response surface and contour plots illustrating the interactive influence of CS ratio (A), applied voltage (B), and feed rate (C) on the fiber diameter of electrospun NFs. The contour plots clearly show that increasing the CS ratio and feed rate led to a progressive increase in fiber diameter. Li and Xia[53] (2004 reported that an increase in polymer concentration or viscosity results in thicker NFs due to reduced elongation of the electrospinning jet. At higher polymer concentrations, the solution viscosity increases due to enhanced chain entanglement and intermolecular interactions. This increased viscosity resists the stretching forces induced by the applied electric field, thereby reducing jet elongation during electrospinning. As a result, the fibers formed are thicker.[53,54] In contrast, higher voltage exerted the opposite effect, reducing

Table 3. Experimental design matrix with independent variable and dependent responses.

Std	RUN	Space type	Factor 1	Factor 2	Factor 3	Response 1	Response 2
			A: Chitosan ratio	B: Voltage	C: Feed rate	Fiber diameter	Tensile strength (MPa)
				kV	µl/hr	nm	MPa
1	1	Factorial	1	18	0.5	262.105	2.2
3	2	Factorial	1	21	0.5	173.142	2.33
11	3	Axial	2	16.9773	1	267.224	1.56
2	4	Factorial	3	18	0.5	265.105	1.27
7	5	Factorial	1	21	1.5	244.575	1.84
12	6	Axial	2	22.0227	1	238.21	1.74
14	7	Axial	2	19.5	1.8409	355.645	1.092
15	8	Center	2	19.5	1	262.105	1.75
13	9	Axial	2	19.5	0.159104	254.128	1.99
6	10	Factorial	3	18	1.5	322.644	0.986
9	11	Axial	0.318207	19.5	1	181.567	2.56
16	12	Center	2	19.5	1	254.117	1.901
5	13	Factorial	1	18	1.5	284.684	1.74
17	14	Center	2	19.5	1	263.384	1.8
10	15	Axial	3.68179	19.5	1	298.11	0.967
4	16	Factorial	3	21	0.5	279.635	1.54
8	17	Factorial	3	21	1.5	375.516	1.11

the diameter and thereby improving the stretching forces of the electrospinning jet. Additionally, higher viscosity limits jet instability and whipping, further contributing to the formation of uniform, but larger, fibers.[55]

Specifically, the A-B interaction revealed that fiber diameter decreased with increasing voltage but increased with higher CS concentration. The B-C interaction further confirmed that higher feed rates favored the formation of thicker fibers, whereas voltage continued to reduce the diameter. Similar findings were observed: higher feed rates supply more solution to the jet, leading to insufficient stretching and, consequently, larger fiber diameters. Similarly, the A-C interaction highlighted a positive correlation among the two parameters and fiber thickness. These findings were further validated by the corresponding 3D surface plots, which depicted smooth response surfaces confirming the trends. Collectively, the analysis indicates that thinner fibers can be obtained at lower CS ratios, higher applied voltage, and reduced feed rates. In contrast, thicker fibers are produced under opposite conditions, as finalized by SEM images of the highest and lowest values of the dependent and independent variables (Figure 1c). In terms of mathematics, it is expressed as:

$$Y1\ (\text{NF diameter}) = 259.24 + 34.74A - 8.09B + 30.62C + 24.5AB + 7.43AC + 10.90BC - 4.92A^2 - 0.3637B^2 + 18.08C^2 \quad \text{(viii)}$$

Effect of input variables on MPa

The MPa of the B-NF was recorded in the range of 0.8 to 2.7 MPa, depending on the values of the independent and dependent variables. The lowest strength (0.967 MPa) was observed for run 16, whereas the strongest bond (2.56 MPa) was observed for run 11. A quadratic model was used to depict the effect on MPa, which effectively determined the correlation coefficient. Figure 1b presents contour plots and a response surface illustrating the combined effects of CS ratio (A), applied voltage (B), and feed rate (C) on MPa. The results indicate that higher CS ratios and feed rates negatively affected MPa, whereas the applied voltage exerted a relatively mild synergistic effect. The decrease in MPa at higher CS ratios can be attributed to increased rigidity and reduced flexibility of the polymeric network, leading to structural inhomogeneity and weaker fiber integrity. Similarly, higher feed rates can result in insufficient solvent evaporation and poor fiber consolidation, thereby reducing mechanical strength. In contrast, increasing the applied voltage improves fiber alignment and stretching, thereby enhancing molecular orientation within the fibers and increasing MPa. However, excessively high voltage may induce jet instability, limiting further improvement.[56]

The contour lines' curved and elliptical shapes demonstrate that curvature, rather than a linear trend, controls the response, confirming the presence of significant quadratic interactions.

A perfect balance of feed rate, CS ratio, and voltage maximizes MPa, and this is the projected optimum, symbolized by a stationary point in the red-marked area. In terms of mathematics, it is expressed as:

$$Y2\ (MPa) = 1.82 - 0.4308A + 0.0678B - 0.2324C + 0.0205AB + 0.0295AC - 0.0220BC - 0.0221A^2 - 0.0623B^2 - 0.1008C^2 \quad \text{(ix)}$$

Final process optimization

The Design-Expert software optimization module was used to minimize Y1 and maximize Y2. Each variable was kept within a specified limit for this purpose. Based on numerical optimization using the CCD model, the optimized formulation parameters were predicted as follows: CS ratio (A) = 2% w/v, applied voltage (B) = 20 kV, and feed rate (C) = 1 µL/hr. Under these conditions, the predicted NF diameter and MPa were 256.504 ± 7.29 nm and 1.833±0.08 MPa, respectively. Table 5 presents the MPa experimental and anticipated findings for NFs under optimal conditions, which align with the observed values. Once the optimized formulation was obtained, 10 mg of the drug was loaded into the final formulation for further characterization.

Table 4. Computed coefficients, model, *p*-values, and fitting statistics of two responses using ANOVA according to CCD used for blank nanofiber optimization.

Response	Y1 (nanofiber diameter)	Y2 (tensile strength)
Intercept	+259.24	+1.82
A	+34.74	-0.4308
B	-8.09	+0.0679
C	+30.62	-0.2324
AB	+24.56	+0.02025
AC	+7.43	+0.0295
BC	+10.90	-0.0220
A^2	-4.92	-0.0221
B^2	-0.3637	-0.0623
C^2	+18.08	-0.1008
R^2	0.9911	0.9871
R^2 predicted	0.9389	0.9193
R^2 adjusted	0.9797	0.9703
SD	7.29	0.0805
CV %	2.70	4.82
Model F value	86.81	59.61
Model *p*-value	< 0.0001	< 0.0001
Model suggested	Quadratic	Quadratic

ANOVA, analysis of variance; CCD, central composite design; SD, standard deviation.

SEM

Figure 2 (a and b) visually represents the comparative SEM micrographs of B-NFs (optimised by CCD) and Ofx-NFs with their mean diameters and frequency distribution histograms. The FESEM characterization data showed that the Ofx-loaded NFs had a consistent, smooth, and nonwoven shape. Furthermore, the surface morphology of the Ofx-loaded NFs was cylindrical, like the NFs, and somewhat entangled in some areas. No drug crystals were visible on the surface of the NFs, indicating that Ofx was evenly distributed within the polymeric NFs. Additionally, compared to B-NFs without Ofx, the average fiber diameter of Ofx-NFs was 187.1±12.87 nm, a decrease in fiber diameter in a range of 120 nm to 50 nm. The decrease in fiber mean diameter upon the addition of Ofx may be ascribed to the enhanced conductivity of the polymer solution following the inclusion of Ofx.[57]

Swelling index

An agar plate technique was used to assess the stability of PVA/CS NF patches over 24 hours. Over the first 8 hours, the swelling behavior of B-NFs increased rapidly, peaking at about 120%. The swelling leveled off at about 100% after a day. The hydrophilic properties of PVA/CS and CS's exceptionally high-water retention, which promote fluid absorption, are responsible for this rise. The polymer network's slight degradation and structural relaxation are probably the causes of the subsequent decline.[58] The swelling trend of drug-loaded NFs was slower, stabilizing at around 105% after 20 to 24 hours and reaching approximately 95% at 8 hours (Figure 2c). This reduced initial swelling suggests that Ofx was incorporated into the polymer chains, forming hydrogen-bonded interactions that provide long-term structural stability while temporarily preventing water penetration. Because it facilitates controlled release by keeping the polymer matrix wet while gradually releasing the drug, its stability is highly beneficial for localised drug delivery.

MPa

Tensile testing was used to assess the mechanical characteristics of both unloaded and drug-laden NF mats (crosshead speed: 5 mm/min, 18 °C). The blank mat's yield strength was 1.99 ± 0.14 MPa, its elongation rate was 17%, its Young's modulus was 16.921 MPa, and its maximum load was 11.15 N. The Ofx-NF mat MPa (1.32 ± 0.08 MPa), elongation rate (13%), and Young's modulus (7.7 MPa) were found to be decreased after drug loading, keeping the maximum load (11.09 N) constant (Figure 2d). This suggests that the integration of the active moiety within the fiber compromises and reduces toughness,[59] possibly owing to enhanced porosity, microstructural imperfections or specific plasticization.[60] As drug loading resulted in a ~56% decrease

Table 5. Illustrates the predicted and observed values of the PVA/CS nanofiber.

Responses (blank nanofiber)	Actual	Predicted
Nanofiber diameter (nm)	244.60 ± 14.21	256.504 ± 7.29
Tensile strength	1.99 ± 0.14	1.833 ± 0.08

PVA, polyvinyl alcohol; CS, chitosan.

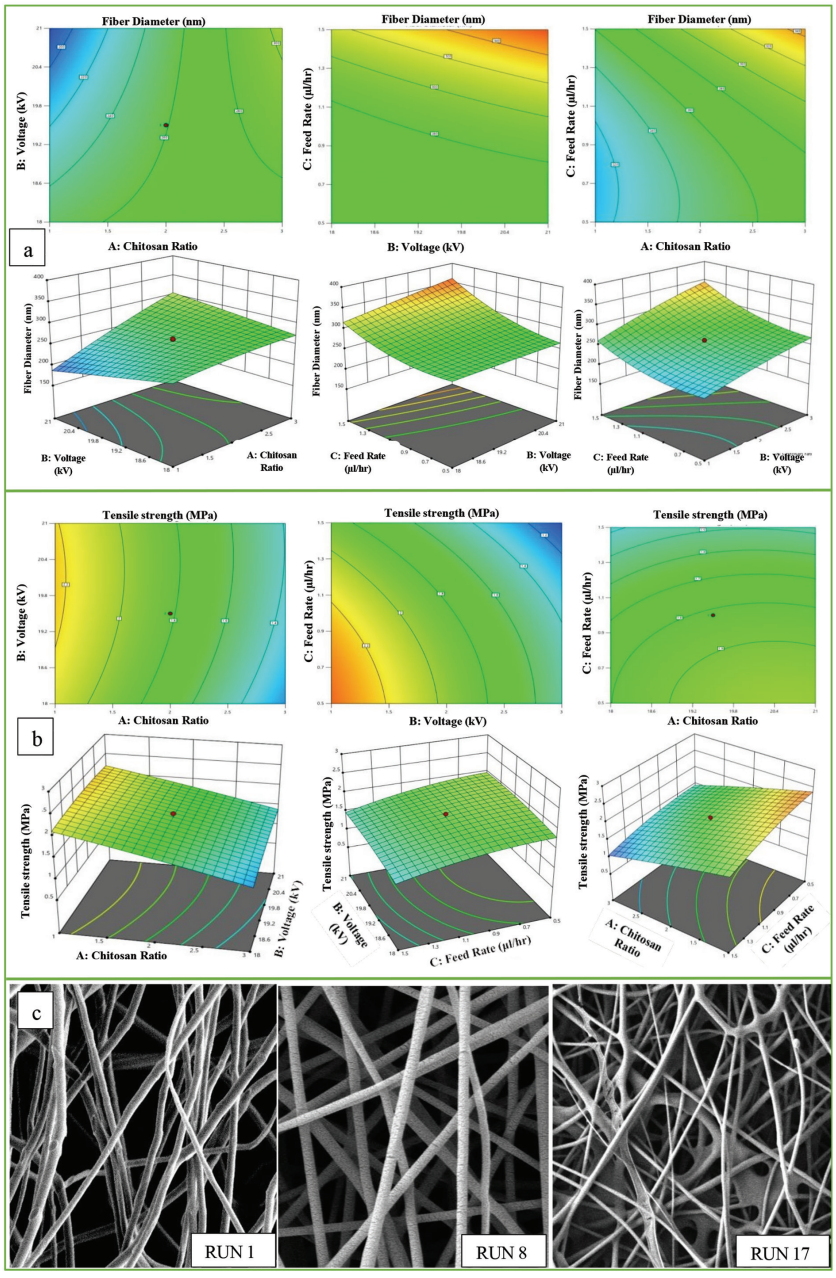

Figure 1. a, b) Contour and 3D response graph effect of the independent variable nanofiber diameter (nm), tensile strength (MPa), respectively. c) SEM images of 1,8 and 17 run numbers used in the design experiment show the nanofiber's quality and density with a 200–400 nm diameter.

SEM, scanning electron microscopy.

in stiffness, a ~41% decrease in MPa, and a ~34% decrease in elongation when compared with blank mats.

FTIR

To observe chemical changes or interactions between the drug and excipients, a FTIR study was performed. The FTIR spectra of the active moiety Ofx, PVA, CS, B-NF, and Ofx-NFs are depicted in Figure 3a. The existence of distinctive peaks of Ofx at 3426 cm^{-1} is due to N-H stretching of the secondary amine group, C = O stretching of carboxylic acid at 1720 cm^{-1}, 1620 cm^{-1} (C = O stretching of the quinolone group), 1287 cm^{-1} (CN stretching), and 1057 cm^{-1} (C-F stretching). PVA showed distinctive absorption bands highlighting a broad peak at 3426 cm^{-1}, indicating OH stretching brought by intermolecular hydrogen bonding, 2428 cm^{-1} (CH stretching), and 1080–1140 cm^{-1} (CO, acetyl groups). At approximately 3469 cm^{-1} (OH and NH stretching), 1650 cm^{-1} (amide I, CO stretching), and 1560 cm^{-1} (amide II, NH bending), CS exhibited distinct peaks. The strong peaks of both polymers were observed in the B-NFs spectra, with minor shifts and decreased intensities, indicating interactions and hydrogen bonding between PVA and CS. The main Ofx characteristic

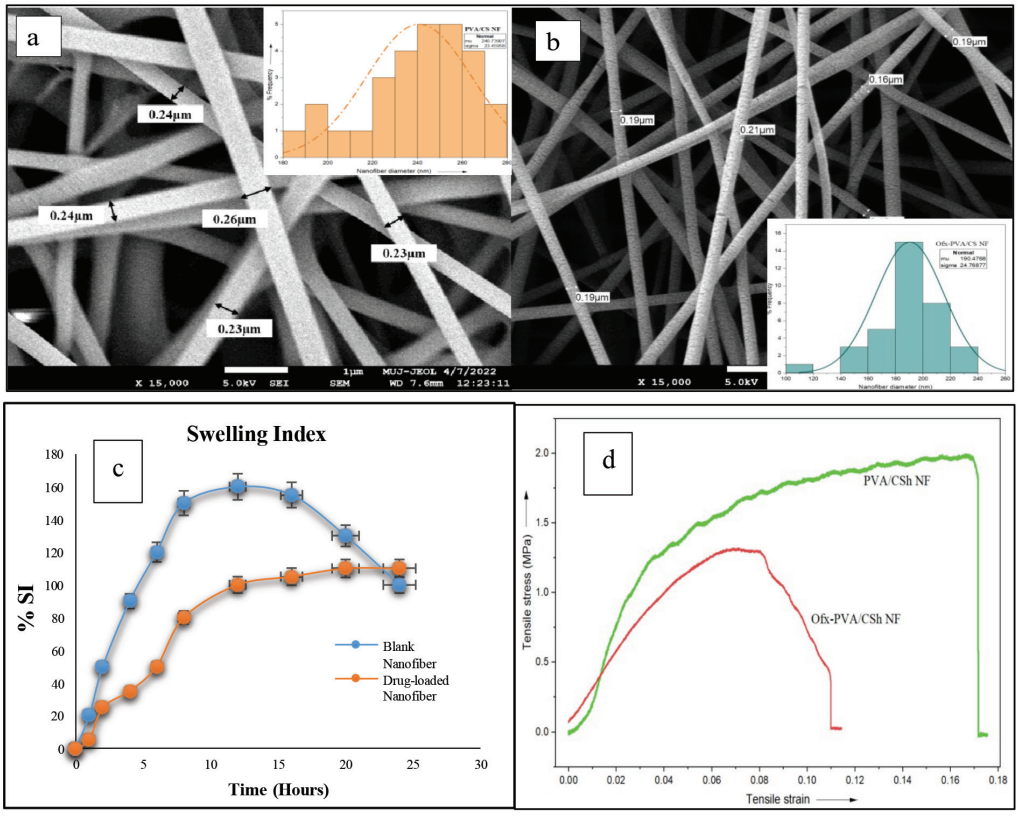

Figure 2. SEM image and frequency distribution curve of a) B-NF (optimised via CCD), b) Ofx-loaded NF; comparative graph of, c) Swelling index, and d) Tensile strength of both the formulations.

Ofx, ofloxacin; PVA, polyvinyl alcohol; CS, chitosan; NF, nanofiber; SEM, scanning electron microscopy; CCD, central composite design.

peaks were visible in the Ofx-NFs spectra, albeit slightly shifted or with diminished strength. This shows that the active moiety was successfully incorporated within the polymeric NF matrix without experiencing any notable disintegration or chemical reactivity. The lack of additional peaks suggested that the drug was loaded primarily through physical trapping and hydrogen bonding, rather than covalent chemical bonding.

DSC

Differential scanning calorimetry was used to determine the thermal properties of Ofx-NF and its constituent parts. Figure 3b shows the DSC temperature maps of Ofx, PVA, CS, B-NFs, and Ofx-NFs. As shown, OFX exhibits a distinct endothermic peak at 276.36 °C, attributed to the melting of the drug and indicating the substance's crystallinity. At approximately 72.81 °C, PVA exhibited an extended endothermic peak, indicating moisture loss. This was promptly followed by a thermal transition indicative of its semi-crystalline structure at 223.05 °C. At 87.35 °C, CS showed an endothermic peak ascribed to structural relaxation and dehydration. Endothermic transitions were observed in the B-NFs at 72.81 °C and 223.05 °C, indicating partial disruption of crystallinity and polymer mixing. Pure Ofx did not exhibit a prominent melting peak, indicating that the drug was successfully entrapped in the polymeric matrix in an amorphous or molecularly dispersed condition. In contrast, the Ofx–PVA/CS NF had peaks at 72.81 °C and 232.75 °C. These results show that Ofx and the PVA/CS network exhibit significant intermolecular interactions, thereby enhancing the formulation's heat stability.[61]

Drug loading and % EE

The theoretical content of the drug in a 2 × 2 cm^2 sample of NFs was calculated to be about 0.25 mg. The drug content obtained was about 0.244 mg, corresponding to an encapsulation efficiency of 97.54 ± 0.89% (n = 3). The drug load in the NFs was 4–7%, depending on the weight of the NF sample. This indicates that nearly all of the active moiety incorporated during electrospinning was effectively retained within the NF matrix, resulting in efficient drug delivery. Appropriate drug loading and higher entrapment of Ofx within the NFs appear capable of providing prolonged and efficient release of it, making them suited for a localized drug delivery system.

In vitro drug release and kinetics

According to the findings, NFs can regulate drug release for up to 216 hours (Figure 4a). The crosslinked Ofx-NFs showed 95.61% drug release over 216 hours, and Ofx alone showed nearly 97% release within 12 hours in SUF at pH 6.8.

An initial burst release of approximately 29% was observed within the first 2 hours, likely due to rapid drug release from the

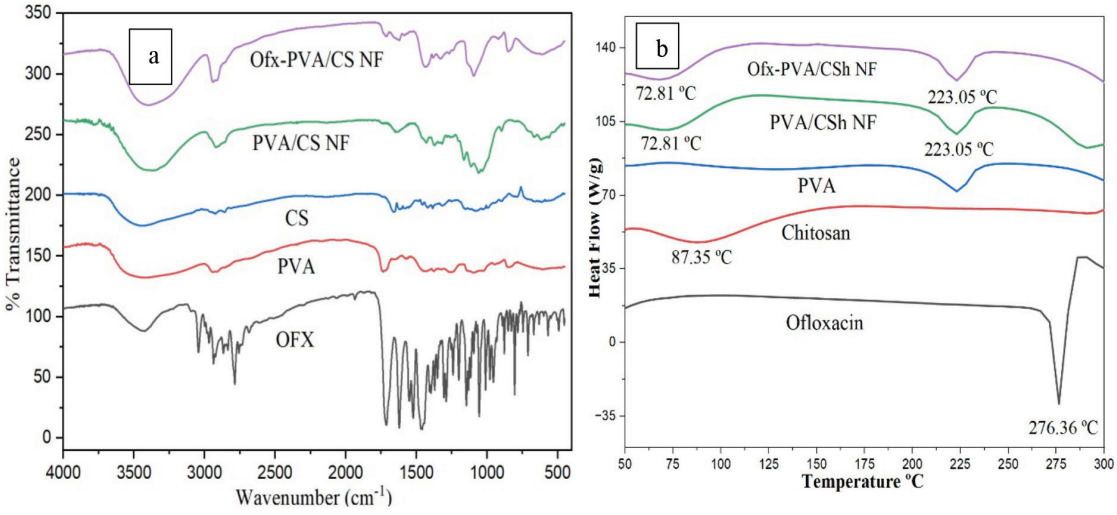

Figure 3. a) FTIR spectra and b) DSC curve of ofloxacin, polymers alone, blank nanofibers, and drug-loaded nanofibers.

Ofx, ofloxacin; PVA, polyvinyl alcohol; CS, chitosan; NF, nanofiber; FTIR, Fourier-transform infrared spectroscopy; DSC, differential scanning colorimeter.

NF surface. This was followed by a sustained-release phase, indicating controlled drug diffusion from the polymeric matrix.

The key factor influencing how long the Ofx remained on the NF was crosslinking the fiber with glutaraldehyde for 24 hours. When PVA/CS NFs are immersed in uterine fluid, they dissolve instantly into a substance comparable to a gelatinous compound.[59] This may limit the application of a PVA/CS coating in uterine tissues. The mechanical properties were improved due to the link created between the reactive side groups of CS (NH) and PVA (OH), achieved by chemical crosslinking with GA vapour.[62] The GA caused the reaction to move from the exterior layer to the interior layer of NF. Therefore, the resulting intermolecular pressures cause both the swelling pace and the pharmaceutical delivery rate to decrease.[37]

Four different mathematical models, along with their corresponding regression values, were employed to describe the release kinetics of Ofx and its release from NFs, as listed in Table 6.

Table 6. Regression coefficient values of the different drug release models.

Model	Ofloxacin	Ofx-NF
Zero order	0.1138	0.113
First order	0.8308	0.2717
Higuchi model	0.9062	0.9062
Korsmeyer–Peppas	0.9492 (n=0.383)	0.9647 (n = 0.236)

Ofx, ofloxacin; NF, nanofiber.

Four distinct mathematical models were employed to explain the release kinetics of Ofx and its release from NFs. However, the Korsmeyer–Peppas model fitted the curves of Ofx (R^2 = 0.9492, n = 0.383) and Ofx Nf (R^2 = 0.9647, n = 0.236) very well, indicating a release mechanism regulated by Fickian diffusion. The dissolution mechanism in both instances was primarily controlled by diffusion through the hydrated polymeric medium, as further demonstrated by the strong correlation with the Higuchi model (R^2 = 0.9062). The first-order (R^2 = 0.8308 and 0.2717) and zero-order (R^2 = 0.1138 and 0.113) models did not fit the data well, suggesting that the release was neither concentration-dependent nor occurring at a steady rate over time. Instead, drug-polymer interactions, hydration, and swelling affected the release. Crucially, Ofx's diffusion rate was decreased when it was incorporated into the PVA/CS NF matrix as opposed to when it was pure, indicating a sustained release behaviour of the drug delivery system.[63,64]

Ex vivo permeation

A sustained release of the active moiety was found to be released across the uterine mucosa of a goat in the *ex vivo* permeation testing. The cumulative permeation profile (Figure 4b) reveals an initial lag phase, followed by a linear rise, and ultimately forms a plateau. Normalization versus membrane surface area was compared by the cumulative amount penetrated per unit area. The computed steady state flux (J) and apparent permeability coefficient (Papp) were 1.027 µg/cm^2/h and 0.01027 cm/h, respectively. These results correlate well with the sustained release profile, indicating that prolonged drug availability from the NFs supports continuous permeation across the mucosal barrier.[65]

It is worth noting that preserved mucosal samples in formalin were used in this experiment; therefore, the natural permeability might be affected by protein cross-linking and decreased fluidity of cell membranes. Thus, the presented outcomes can only be considered relative rather than actual data, since the

permeability of living tissues may differ. Identical results were achieved during multiple tests under the same conditions.

Mucoadhesion study

Using the manual modified glass-slide method, the mucoadhesive strength of the composed fiber was assessed on goat uterine mucosa. The detachment force and residence duration of B-NF were 0.72 ± 0.13 N and 65 ± 0.8 min, respectively, while drug-loaded had somewhat lower values (0.45 ± 0.14 N; 40 ± 0.15 min). This decrease in the range is explained by Ofx molecules interfering with the hydrogen bonding between polymers and mucin, which weakens adherence.[66] NF formulations maintained strong adherence due to their large surface area, porous structure, and close penetration into the mucosal folds, which improve physical entanglement and adhesive interactions.[67]

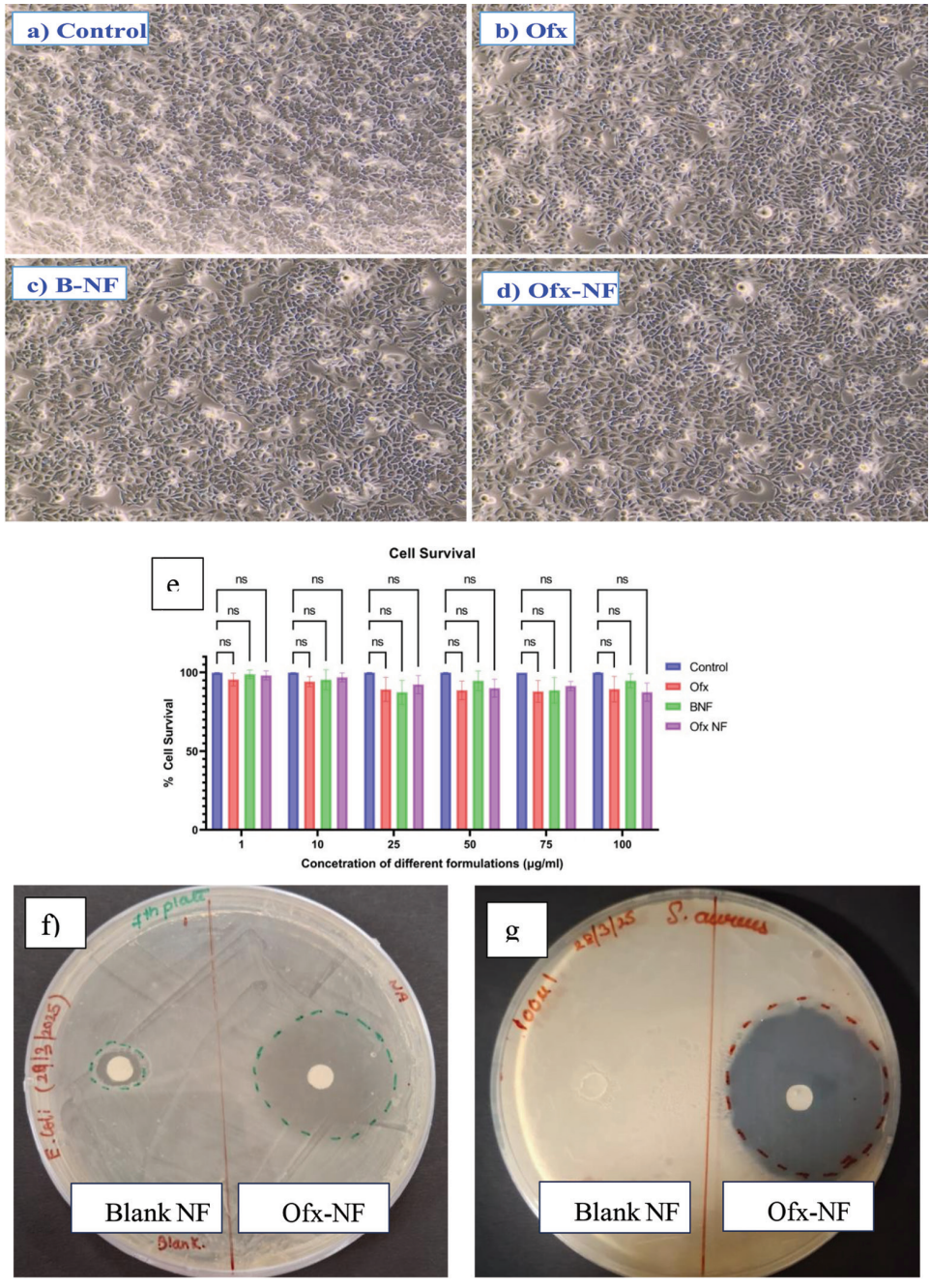

Figure 4. *In vitro,* (a-e) cell viability performed on HeLa cells after being treated for 24 h under a 40× inverted microscope: (a) control (DMSO), (b) Ofx, (c) B-NF, (d) Ofx-NF (100 µg/mL Conc.), and (e) graphical representation of % cell viability v/s drug and formulation at different concentrations (ns = statistically non-significant, $p > 0.05$) (f, g) antimicrobial study showing zone of inhibition on f) *E. coli* g) *S. aureus.*

Ofx, ofloxacin; NF, nanofiber; B-NF, black NF.

Cell viability study

The cytotoxicity test was used to determine cell viability of Ofx, B-NF, and Ofx-NF at doses ranging from 1 to 100 µg/mL against HeLa cells, and was evaluated by microscopic observation. All examined groups remained viable (> 90%), and there was no discernible difference between the Ofx, B-NF, and Ofx NF groups. Adding Ofx did not result in cytotoxic effects, and the NF matrix was non-toxic. Using DMSO as a control, microscopic pictures of the treated cells were taken at a concentration of 100 µg/ml (Figure 5a). Neither the B-NF nor Ofx-NF exhibited any cytotoxic effects on HeLa cells when observed under a microscope. Cell viability was somewhat lower in pure Ofx at a 100 µg/ml dose. Figure 5e also shows the cytotoxic effects of several samples as a percentage plot of cell viability against concentration. Since there was no discernible 50% decrease in cell viability, the IC_{50} values for Ofx, B-NF, and Ofx NF were more than 100 µg/mL, respectively. Although cell viability reveals a negative impact on increasing the concentration for all treatment groups (Ofx, B-NF, and Ofx NF), statistical analysis using two-way ANOVA followed by Dunnett's multiple comparison test revealed that the changes were not statistically significant (NS) ($p > 0.05$). These findings indicate that the developed nanoformulations exhibit good cytocompatibility and do not significantly affect mammalian cell viability under the studied conditions.

Antimicrobial study

Using the disc diffusion agar method, the effectiveness of Ofx, NF, and Ofx-NF was evaluated against Gram-positive and Gram-negative bacteria (i.e., *S. aureus* and *E. coli*). Figure 5f and Figure 5g displays the antibacterial performance of each sample. The presence of innate antibacterial activity was confirmed by the B-NFs and Ofx-NFs exhibiting a 5 ± 1.68 mm and 25 ± 0.65 mm zone of inhibition (ZOI) in *E. coli*, respectively, in Figure 5f. The *S. aureus* culture plate in Figure 5g showed no ZOI by B-NFs, but the ZOI for OFX-NFs was 35 ± 0.08 mm. Due to the drug's rapid accessibility in the medium, the drug-loaded NFs exhibited the largest ZOI, indicating strong antibacterial capabilities. Detecting an inhibitory zone in the NF blank in *E. coli* demonstrates that OFX-NFs function as a synergistic system. The presence of CS with antibacterial qualities, which results from the regulated release of the active moiety from the confined extracellular matrix of the NF, may be the source of this.[68]

In vivo study

Isolation and identification of bacteria

To identify and isolate bacteria from the uterus of cattle with SE, a sample must be aseptically collected using cytobrush technology. MLA, BHI, SDA, and other selective and nonselective media are inoculated with the sample and incubated under the appropriate conditions. A critical step in identifying bacteria is the Gram stain technique, which distinguishes bacteria based on the arrangement of their cell wall's membrane.

Under a microscope, Gram-negative bacteria, such *as E. coli*, absorb the contrast dye (safranin), making them appear pink (Figure 6a), whereas Gram-positive bacteria, such as *Staphylococcus* species, retain the crystal violet pigment and appear purple (Figure 6b).[69] *E. coli* was the most frequently isolated bacterium, followed by *Staphylococcus* spp., a hybrid infection (gram-positive and gram-negative rods), and *Candida* spp. The outcomes were analysed using statistics, and it was found that *E. coli* was a ubiquitous bacterium isolated from the uteri of the cattle under research.[70] Meanwhile, the incidence of *Staphylococcus* sp. and a combined infection was also documented. Only *Candida* spp. was detected in uterine samples (Figure 6c).

Effect of treatment on bacterial load of uterine lavage samples

The impact of therapy on the number of microorganisms present in uterine lavage samples was analyzed during oestrus. In Group 1 (control), normal saline was administered, and a slight reduction in CFU/mL was observed; however, this was not statistically significant, as it was similar to the pretreatment levels in Groups 2 and 3. In groups 2 and 3, the CFU count

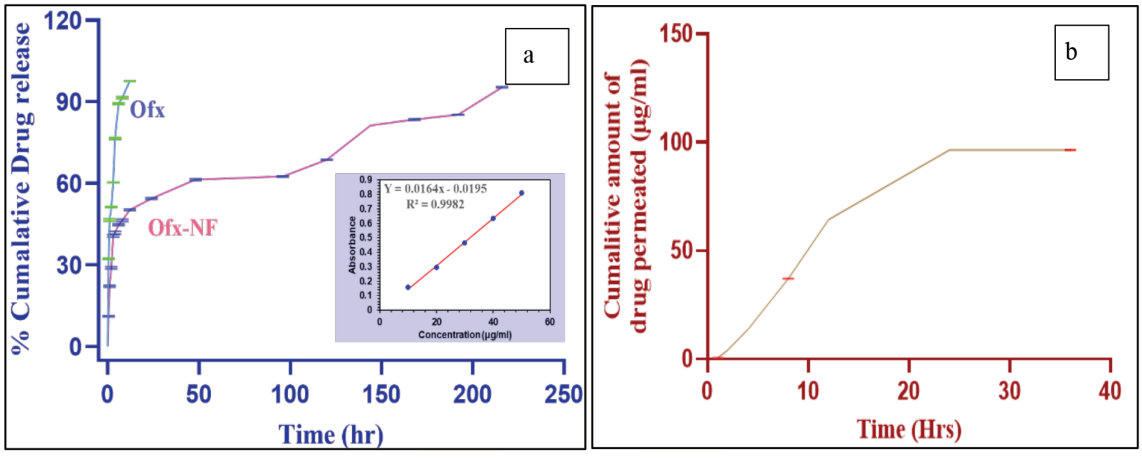

Figure 5. Graphical representation of a) *in vitro* release and b) *ex vivo* permeation studies of Ofx from Ofx NFs.
Ofx, ofloxacin; NF, nanofiber.

decreased significantly ($p \leq 0.05$) post-treatment, even though the values were numerically lower in group 3 than in group 2; however, this difference was not significant ($p \leq 0.05$), as depicted in Table 7.

pH of vaginal mucus

The pH of cervicovaginal mucus in the control and treatment group (Ofx, Ofx-NFs) was recorded during oestrous. No significant difference ($p < 0.05$) was recorded between the mean pH value of cervicovaginal mucus of the control group and the positive control group, both at the pre-treatment and post-treatment stages. A significantly ($p < 0.05$) higher mean pH value of cervicovaginal mucus was observed in the Ofx-NF-treated group as compared to the positive control group after post-treatment (Table 7).

Endometrial cytology for the diagnosis of SE

The proportion of PMN cells, a marker of infection or inflammation, was assessed in three groups: the positive control group (group 2; Ofx-treated group), the control group (normal saline), and the Ofx-NFs group (Table 7) before and after treatment. In groups 2 and 3, significant reductions in PMNs ($p \leq 0.05$, one-way ANOVA) were observed both before and after treatment. The PMN count was lower in group 3 than in group 1, but the difference was not significant. Post-treatment, PMN cells decreased significantly in both groups 2 and 3; however, the incorporation of Ofx in NF showed greater effectiveness (Figures 7a and 7b). The Ofx-NF treatment was found equally efficient as that of Ofx even at 1/3rd doses (total 400 mg intrauterine) and single administration, compared to that of Ofx, given at comparatively high doses, i.e., total 1200 mg, which was administered for 3 days in divided doses (conventional treatment, i.e., 400 mg daily intrauterine), suggesting sustained release potential of the Ofx-NF.

Pregnancy diagnosis

Pregnancy rates in Groups I, II, and III were evaluated following artificial insemination during the subsequent estrus. The highest pregnancy rate was observed in Group III (Ofx-NF), followed by Group II, while the lowest was recorded in Group I (control) (Figure 7c). The differences among groups were statistically significant ($p < 0.05$, chi-square test). However, none of the animals in group 1 conceived, as previously reported, indicating

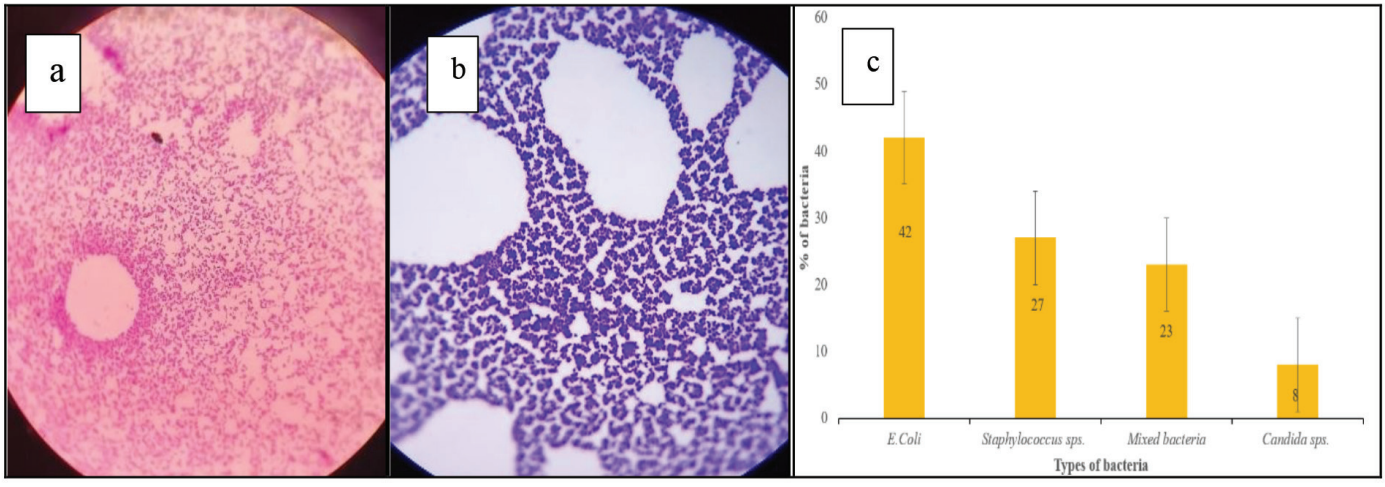

Figure 6. Microscopic image of a) *E. coli*, b) *Staphylococcus* spp. and c) graphical representation of identified types of bacteria in uterine samples.

Table 7. Effect of bacterial load in uterine samples, pH of cervicovaginal mucus in cattle, PMN cells, and pregnancy status of experimental animals (n = 8).

Type of treatment	Pre/post treatment	Group 1 (Control)	Group 2 (positive control)	Group 3 (nanofiber)
Effect of bacterial load	Pre	$2.33\times10^5 \pm 47.06^A$	$2.32X10^5 \pm 89.57^A$	$2.33X10^5 \pm 70.21^A$
	Post	$2.31X10^5 \pm 71.23^A$	$2.32X10^3 \pm 12.09^B$	$1.23X10^3 \pm 20.86^B$
pH of cervicovaginal mucus	Pre	7.13 ± 0.09^A	7.52 ± 0.7^A	7.2 ± 0.7^A
	Post	7.28 ± 0.06^A	7.92 ± 0.1^A	8.2 ± 0.9^B
PMN cells	Pre	7.57 ± 0.35^A	7.52 ± 0.29^A	7.66 ± 0.61^A
	Post	7.73 ± 0.36^A	2.50 ± 0.32^B	1.83 ± 0.30^B
Pregnancy outcome	Post	8 not conceived	4 pregnant	4 pregnant

Data in an identical row containing various superscripts vary considerably ($p \leq 0.05$).
PMN, polymorphonuclear cell.

that SE severely impacts reproductive performance.[71] The NF was equally effective in treating SE, even at one-third the dose of the conventional treatment regimen. Thus, the NF-treated group achieved the highest pregnancy rates after insemination (Table 7). It was found that vaginal pH also affects the rate of conception.[72] Thus, pH estimation can be an alternative, non-invasive method for tracking cattle fertility and uterine health. While values around pH ≥ 8.0 are substantially associated with better conception and pregnancy outcomes, a threshold of pH ≥ 7.0 is a reliable predictor of SE.[73] Similar results support the use of vaginal pH monitoring as a reliable measure for both early disease identification and reproductive performance prediction, despite slight discrepancies across studies due to methodological variables.[74]

Pharmacokinetic study

Ofx concentrations in plasma samples were quantified using an RP-HPLC method. A calibration curve was constructed over the concentration range of 2-10 µg/mL, showing good linearity (R^2 = 0.998). The LOD and LOQ were 0.54 µg/mL and 1.65 µg/mL, respectively.

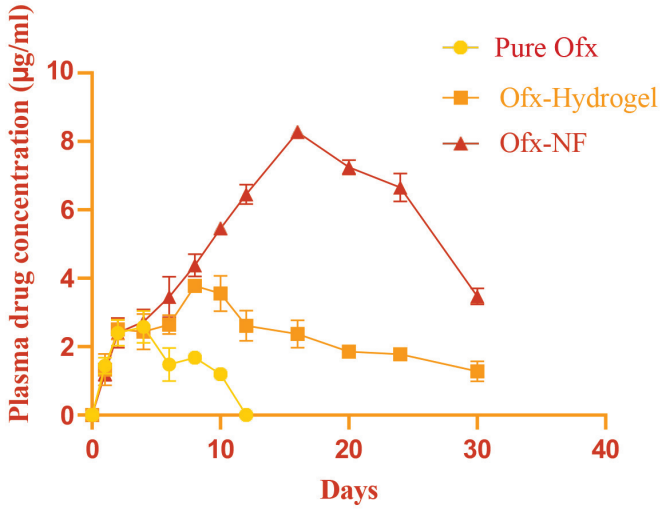

Figure 7. Plasma concentration time graph of drug and formulations.
Ofx, ofloxacin; NF, nanofiber.

Ofx, Ofx-hydrogel (taken for a comparative study), and Ofx-NF were assessed for additional *in vivo* pharmacokinetic research. Figure 8 displays the graph against drug plasma concentration with time. Ofx, Ofx-hydrogel (used for comparative purposes), and Ofx-NF were assessed for additional *in vivo* pharmacokinetic studies. The animals treated with Ofx-NF (Group III) and Ofx-hydrogel (Group IV) exhibited significantly higher plasma drug concentrations at various time points than those treated with pure Ofx (Group I) ($p < 0.0001$; two-way ANOVA).

Pharmacokinetic parameters were calculated using PK Solver software, and the results are summarized in Table 8. Ofx-NF and Ofx-hydrogel exhibited significantly higher mean residence times and C_{max} values than pure Ofx. The clearance rate of the free drug was 10-15 times higher than that of the nanoformulation. This may be due to the high entrapment of Ofx into the nanoformulation, resulting in a low volume of distribution for Ofx-NF/Ofx-HG. The significance of the pharmacokinetic factors makes it clear that the production of Ofx (400 mg: dose at once) in the form of NF resulted in a sustained effect with a higher T_{max} value and MRT, with a lower volume of drug distribution in comparison to pure Ofx (cumulative dose of 1200 mg : 400 mg for 3 consecutive days), which resulted in lower MRT, T_{max} with higher clearance rate. These outcomes reinforce Ofx-NF as a potential drug delivery system, extending the drug's biological half-life and increasing its bioavailability.[37] These favorable data may suggest greater efficacy and the potential for dose reduction in veterinary treatment.

DISCUSSION

The goal of the current study was to develop and statistically optimize Ofx-loaded PVA/CS NF via a CCD approach to deliver intrauterine in bovines during SE. This model enabled the systematic evaluation of formulation variables, such as the effect of the polymer (CS), applied voltage, and flow rate, on critical quality attributes, including fiber diameter and MPa. The statistical analysis indicated a quadratic fit model for both responses, with regression coefficient values (R^2) of 0.979 and 0.970 for NF diameter and MPa, respectively.

Table 8. Various pharmacokinetic parameters.

Parameter	Unit	Ofx	Ofx-hydrogel	Ofx-nanofiber
$t_{1/2}$	D	4.54 ± 2.57	12.03 ± 1.93	9.39 ± 3.25
T_{max}	D	2 ± 1.07	10 ± 0.57	16 ± 1.12
C_{max}	µg/mL	2.68 ± 1.27	3.92 ± 2.97	8.14 ± 1.98
$AUC_{0-\infty}$	µg/mL*d	21.82 ± 2.46	86.60 ± 1.62	215.28 ± 1.63
MRT	D	7.55 ± 1.03	20.35 ± 1.82	22.83 ± 2.51
Vz/F	(mg)/(µg/mL)	180.68 ± 0.52	40.11 ± 2.29	12.59 ± 1.05
Cl/F	(mg)/(µg/mL)/d	27.49 ± 1.87	2.30 ± 3.99	0.92 ± 0.89

AUC, area under the curve; Ofx, ofloxacin.

The predicted formulation, as per the CCD model, yielded bead-free, smooth, and uniformly sized NFs with an average diameter of 256.504 ± 7.29 nm, as analysed by SEM, and a MPa of 1.833 ± 0.08 MPa, as analysed by the texture analyzer. The minimum discrepancy between the experimental and anticipated values supports the validity of the optimization procedure used in this investigation. The inclusion of the active moiety (Ofx) within the predicted NF structure (CCD) resulted in an overall decrease in MPa and a reduction of NF diameter from 120 nm to 50 nm, due to adequate encapsulation of the drug within the polymeric matrix system. The physicochemical properties of the drug, excipients, and formulation were verified using FTIR and DSC. FTIR reveals no incompatibility between the drug and excipients used in the formulation. In contrast, a slight shift or diminished strength of a sharp peak shows that the active moiety was successfully incorporated within the polymeric NF matrix without experiencing any notable disintegration or chemical reactivity. The absence of a prominent melting point peak of Ofx-NF in the DSC thermogram suggests that the drug is successfully entrapped in the polymeric matrix, either in an amorphous or molecularly dispersed condition. The higher encapsulation efficiency and lower swelling index of Ofx-NF result in efficient drug release. The *in vitro* release studies unveiled burst release of Ofx solution within a few hours, and in the case of Ofx-NF, a sustained release of Ofx from the polymeric matrix for more than 7 days. A polymeric matrix of PVA/CS encapsulated with Ofx acts as a diffusion barrier, enabling a slow release of the molecule. Thus, crosslinking of these PVA/CS NFs with glutaraldehyde may lower the release rate. At the same time, strong electrostatic interactions and hydrogen bonds between both the polymers further contribute to a compact structure that restricts rapid drug diffusion.[75] Furthermore, the Korsmeyer–Peppas kinetic model was well-fitted, suggesting the diffusion of Ofx from the NF through the hydrated polymeric medium. The antimicrobial study revealed that the Ofx-loaded NF effectively inhibited the growth of *E. coli* and *S. aureus*, the predominant pathogens associated with bovine metritis. The observed antibacterial effect can be correlated with the sustained availability of Ofx at the target site, which ensures prolonged exposure of bacteria to the therapeutic concentration of the drug. The mucoadhesive properties of the NF were significantly enhanced by incorporating CS into the PVA matrix. Mucoadhesion testing confirmed strong adherence of the NF to goat uterine mucosa, which is likely due to the cationic nature of CS and its interaction with negatively charged mucin. This property is particularly beneficial for intrauterine application, as it enhances retention time and prevents premature expulsion of the formulation. Similar findings have been reported for PVA/CS-based systems used in vaginal and wound applications.[76] Experiments on the survival of HeLa cells have demonstrated that NFs are non-toxic and biocompatible, maintaining viability of over 80–90% after 24 hours of exposure. The lack of

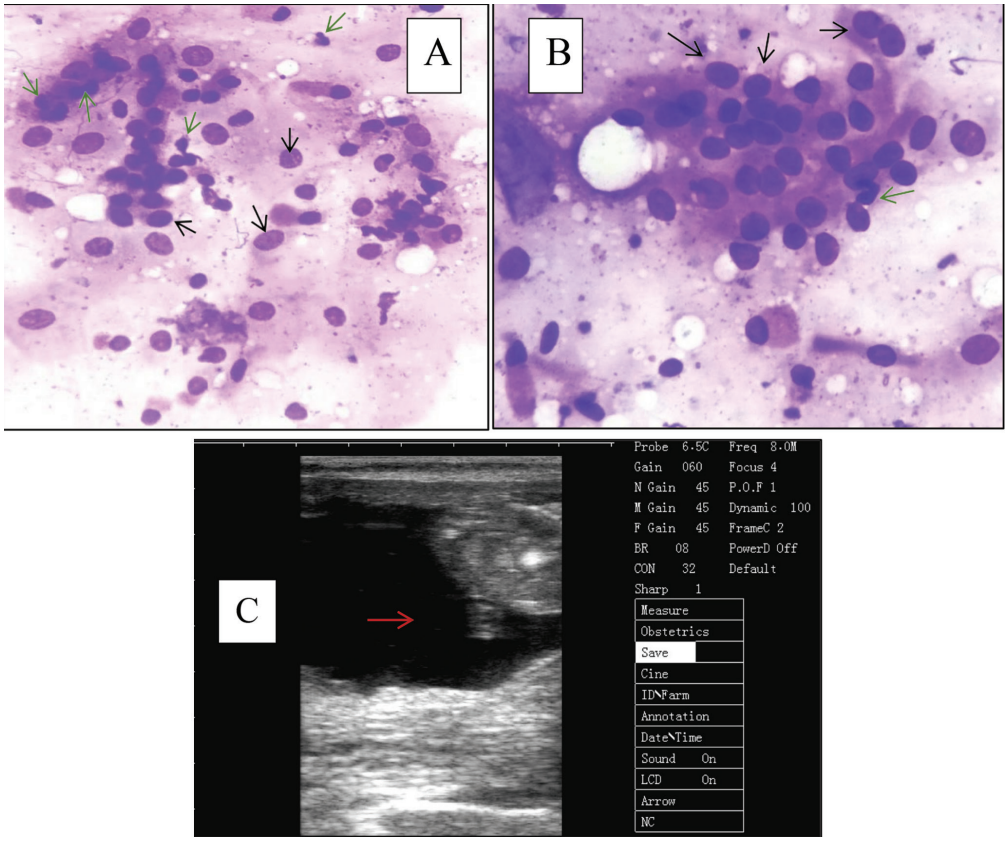

Figure 8. Microscopic picture (40X) of endometrial cytology showing PMNs (green arrows) in between endometrial cells (black arrows) A) pre-treatment b) post-treatment c) ultrasonography image of bovine pregnancy (red arrow showing embryo).

cytotoxicity indicates that both the polymers (PVA and CS) and the incorporation Ofx are suitable for mucosal application. The *ex vivo* permeation investigation with excised goat mucosa revealed a progressive and regulated elimination of Ofx from the NF scaffold. The potential of the NF to maintain drug transport across the uterine epithelium was confirmed by its permeation flux and cumulative drug permeation. The intimate contact of mucoadhesive NFs with the mucosal surface and CS's bioadhesive properties momentarily open epithelial tight junctions, promoting drug diffusion, which may be the cause of the enhanced permeation. However, the present study is not limited to *in vitro* and *ex vivo* evaluations.

Future studies should include *in vivo* pharmacokinetic and pharmacodynamic investigations in bovine models to assess the real-time drug release, local absorption, and therapeutic efficacy. Isolation of bacteria from cattle uterus was identified using staining technique, which indicated the presence of *E. coli* > *Staphylococcus* spp. > mixed bacteria > *Candida* spp. in SE animals. The CFU count revealed a significant difference in Ofx and Ofx NF between treated cattle and controls. A similar result was observed in the case of cervico vaginal pH, which was brought up, i.e., shifting of neutral pH to slightly alkaline. The most crucial pharmacodynamic study to assess SE treatment efficacy is the endometrial cytology study for SE diagnosis. Since PMS cells are recognized as markers of inflammation, a significant reduction in PMN cells was observed after post-treatment with Ofx NF compared to Ofx alone. The conventional treatment involved a cumulative dose of 1200 mg of Ofx (400 mg administered over three consecutive days), whereas the Ofx-NF formulation was administered as a single intrauterine dose of 400 mg. Despite the lower total dose, the Ofx-NF formulation demonstrated comparable therapeutic efficacy, likely due to its sustained-release properties and enhanced local retention at the site of action. This study was designed to evaluate the sustained-release and localized delivery efficiency of the NF system rather than direct dose equivalence. Therefore, the findings should be interpreted in terms of improved drug retention, prolonged release, and localized bioavailability rather than in terms of cumulative dose comparisons. Furthermore, the therapeutic effectiveness was supported by pregnancy outcomes, with the NF-treated group exhibiting a higher conception rate than the conventional Ofx-treated group, indicating improved clinical efficacy of the developed formulation. This suggests that the NF was equally effective in treating SE, even at one-third the dose of the conventional treatment regimen. It was also found that animals with vaginal pH levels of 8 or higher have a higher chance of pregnancy or better conception than those with acidic or neutral pH levels. Thus, vaginal pH evaluation can also serve as an alternative diagnostic tool for identifying SE. A pharmacokinetic study further supported the controlled release and retention behavior of the optimized formulation. Drug concentration-time profiles were compared with those of pure Ofx, Ofx-NF, and Ofx-Hydrogel, which showed notably greater mean residence times and maximum concentrations. The clearance rate of Ofx alone was 10–15 times higher than that of the nanoformulation. This might be due to a lower volume of distribution of the formulation compared to a larger trapping of Ofx within it. Ofx-NF produced prolonged effects, with enhanced T_{max} and MRT, following a single 400 mg dose; however, pure Ofx administered over 3 days resulted in reduced T_{max} and MRT, accompanied by higher clearance.

These results demonstrate that Ofx-NF is a viable drug delivery method that improves the bioavailability and retention of medications in veterinary therapy, leading to enhanced efficacy and potential dose reduction. It sustains therapeutic levels at the target site for an extended period, benefitting clinical outcomes and presenting a cost-effective solution for intrauterine infections. While the development of Ofx-loaded PVA/CS NFs shows promise for localized treatment in bovine uterine infections, further research is required to assess long-term safety and effectiveness.

Study limitations

The present study has some limitations that should be considered when interpreting the findings. The study was conducted using a relatively limited number of animals and under controlled experimental conditions; therefore, the findings may not fully represent the variability encountered in field conditions. Although the developed mucoadhesive nanofiber demonstrated promising therapeutic potential for managing subclinical endometritis, the observation period was limited and did not allow assessment of long-term reproductive outcomes or infection recurrence. Furthermore, comprehensive long-term safety and local tissue tolerance studies are required to establish the safety profile of repeated or prolonged administration. A larger-scale, multicentric field study with extended follow-up and direct comparison with established therapeutic regimens would be valuable to further confirm the efficacy, safety, and practical applicability of the developed nanofiber formulation. Future studies should also investigate its effects on subsequent reproductive performance, calving-to-conception interval, and pregnancy rates under commercial farm conditions.

CONCLUSION

Intrauterine delivery of Ofx-loaded PVA/CS NF was hypothesized to improve the efficacy of Ofx in the treatment of SE in cattle. The encapsulation of Ofx in NFs provides a larger surface when applied at the site of action. The design of localized treatment of bovine endometritis presents a promising advancement in veterinary drug delivery. The incorporation of mucoadhesive polymers such as CS and PVA, along with process parameter optimization through CCD, results in NFs exhibiting desirable mechanical strength, mucoadhesive properties, and controlled drug release profiles. The current data, including both *in vitro* and *in vivo* research, demonstrate an innovative strategy for delivering Ofx via intrauterine NF encapsulation, facilitated by the development of Ofx-NFs. The creation of Ofx-NFs improved Ofx's residence time, increased its t1/2, and enhanced treatment efficiency, even at 1/3rd the doses of the conventional treatment regimen, with optimum pregnancy rates. This could result in a single administration of the formulation during the

entire course of treatment for SEs. The overall performance and cytotoxicity of Ofx against HeLa cells were improved upon encapsulation in the NF, as shown in cell viability studies. This can be investigated further in preclinical studies to confirm and explore.

Advantages over conventional treatments and research gaps

Cattle with SE are frequently treated with systemic or intrauterine antibiotics, including fluoroquinolones, tetracyclines, and cephalosporins. The aforementioned remedies can lower the microbial load. Still, they are often ineffective due to systemic adverse reactions, limited bioavailability at the site of infection, minimal drug retention in the uterine lumen, and the potential for the development of antimicrobial resistance after recurrent administration. Additionally, only a portion of the drug is delivered to the tissue of the uterus in therapeutically beneficial doses via oral or intravenous delivery. Localized delivery methods based on NFs are a viable substitute. With their high drug-loading capacity, regulated release, robust adherence to mucosal surfaces, and enhanced penetration, electrospun NFs, particularly those made with mucoadhesive polymers like CS and PVA, ensure sustained medication availability at the target site. Thus, Ofx-loaded NFs may be able to address several issues with traditional intrauterine antibiotic infusions, such as rapid clearance, medication waste, and suboptimal therapeutic response. Large-scale livestock operations may find localized NF systems appealing for their potential economic benefits, including reduced treatment frequency and easier administration, as well as their improved antibacterial efficacy. Research on veterinary applications is still lacking; nevertheless, significant gaps exist in long-term safety assessments, standardized testing procedures, *in vivo* efficacy studies, and regulatory approval processes for animals used in food production. For Ofx-loaded NFs to be used in veterinary medicine, several issues must be resolved. Ultimately, in bovine SE, localized mucoadhesive NF systems offer a significant opportunity to enhance treatment outcomes, aid in fertility restoration, and mitigate antibiotic resistance.

Ethics

Ethics Committee Approval: All animal experiments adhered to the CPCSEA guidelines and received approval from the IAEC of Sardar Vallabh Bhai Patel University (approval no: IAEC/SVPUAT/2022/109, dated May 24, 2022).

Informed Consent: This study did not involve human participants; hence, patient consent was not required.

Footnotes

Authorship Contributions

Surgical and Medical Practices: P.K., Concept: P.K., A.K.G., Design: P.K., A.K.G., Data Collection or Processing: P.K., A.T., M.K.S., S.P., J.P., R.K.S., G.R., D.D., A.K.G., Analysis or Interpretation: P.K., S.Y., A.T., J.P., R.K.S., G.R., A.K.G., Literature Search: P.K., A.K.G., Writing: P.K.

Conflict of Interest: The authors declare no conflicts of interest.

Financial Disclosure: The author thanks to Department of Biotechnology (BT/PR46598/AAQ/1/938/2022) and the Indian Council of Medical Research (RBMH/FW/2021/9).

REFERENCES

1. Sheldon IM, Cronin J, Goetze L, Donofrio G, Schuberth HJ. Defining postpartum uterine disease and the mechanisms of infection and immunity in the female reproductive tract in cattle. Biol Reprod. 2009;81:1025-1032.
2. Adnane M, Kaidi R, Hanzen C, England GCW. Risk factors of clinical and subclinical endometritis in cattle: a review. Turk J Vet Anim Sci. 2017;41:1-11.
3. Angel QAL, Vigo FM, José BGJ, Barrio LM, José GH, Ana IPMP. Subclinical endometritis in dairy cattle. In: Payan-Carreira R, ed. New Insights into Theriogenology. London; UK; 2018:79-97.
4. Cai XS, Jiang H, Xiao J, Yan X, Xie P, Yu W, Lv WF, Wang J, Meng X, Chen CZ, Zhang M, Zhang Y, Yuan B, Zhang JB. Changes in bacterial community composition in the uterus of Holstein cow with endometritis before and after treatment with oxytetracycline. Sci Rep. 2024;14:9511.
5. Karstrup CC, Pedersen HG, Jensen TK, Agerholm JS. Bacterial invasion of the uterus and oviducts in bovine pyometra. Theriogenology. 2017;93:93-98.
6. Sundrum A. Metabolic disorders in the transition period indicate that the dairy cows' ability to adapt is overstressed. Animals (Basel). 2015;5:978-1020.
7. Wagener K, Gabler C, Drillich M. A review of the ongoing discussion about definition, diagnosis and pathomechanism of subclinical endometritis in dairy cows. Theriogenology. 2017;94:21-30.
8. Di Gennaro F, Guido G, Frallonardo L, Pennazzi L, Bevilacqua M, Locantore P, Vitagliano A, Saracino A, Cicinelli E. Chronic endometritis and antimicrobial resistance: towards a multidrug-resistant endometritis? an expert opinion. Microorganisms. 2025;13:197.
9. Hurtgen JP. Pathogenesis and treatment of endometritis in the mare: a review. Theriogenology. 2006;66:560-566.
10. Hussain AM, Daniel RC. Bovine endometritis: current and future alternative therapy. Zentralbl Veterinarmed A. 1991;38:641-651.
11. Ghimpețeanu OM, Pogurschi EN, Popa DC, Dragomir N, Drăgotoiu T, Mihai OD, Petcu CD. Antibiotic use in livestock and residues in food-a public health threat: a review. Foods. 2022;11:1430.
12. Kasimanickam R, Duffield TF, Foster RA, Gartley CJ, Leslie KE, Walton JS, Johnson WH. The effect of a single administration of cephapirin or cloprostenol on the reproductive performance of dairy cows with subclinical endometritis. Theriogenology. 2005;63:818-830.
13. Alaoui Mdarhri H, Benmessaoud R, Yacoubi H, Seffar L, Guennouni Assimi H, Hamam M, Boussettine R, Filali-Ansari N, Lahlou FA, Diawara I, Ennaji MM, Kettani-Halabi M. Alternatives therapeutic approaches to conventional antibiotics: advantages, limitations and potential application in medicine. Antibiotics (Basel). 2022;11:1826.
14. Hariharan A, Tran SD. Localized drug delivery systems: an update on treatment options for head and neck squamous cell carcinomas. Pharmaceutics. 2023;15:1844.
15. Bassi da Silva J, Ferreira SBS, de Freitas O, Bruschi ML. A critical review about methodologies for the analysis of mucoadhesive properties of drug delivery systems. Drug Dev Ind Pharm. 2017;43:1053-1070.

16. Yao J, Zou P, Cui Y, Quan L, Gao C, Li Z, Gong W, Yang M. Recent advances in strategies to combat bacterial drug resistance: antimicrobial materials and drug delivery systems. Pharmaceutics. 2023;15:1188.

17. Yang Y, Han M, Kong J, Jin Y, Huang Y, Wang J, Li R, Pan Y, Fan J, Li Z. Application of electrostatic spinning technology for oral mucosal drug delivery. AIP Advances. 2025;15:1-12.

18. Hiwrale A, Bharati S, Pingale P, Rajput A. Nanofibers: A current era in drug delivery system. Heliyon. 2023;9:e18917.

19. Maliszewska I, Czapka T. Electrospun polymer nanofibers with antimicrobial activity. Polymers (Basel). 2022;14:1661.

20. Henriques C, Vidinha R, Botequim D, Borges JP, Silva JA. A systematic study of solution and processing parameters on nanofiber morphology using a new electrospinning apparatus. J Nanosci Nanotechnol. 2009;9:3535-3545.

21. Al-Abduljabbar A, Farooq I. Electrospun polymer nanofibers: processing, properties, and applications. Polymers (Basel). 2022;1:65.

22. Shakeri H, Shokrollahi M, Tolabi H, Haghbin Nazarpak M, Solouk A. Design and manufacture of propolis loaded multilayer nanofibrous mucoadhesive patch for the treatment of oral mucosal lesions. J Drug Deliv Sci Technol. 2025;105:106630.

23. Elgharbawy AS, El Demerdash AM, Sadik WA, Kasaby MA, Lotfy AH, Osman AI. Enhancing the biodegradability, water solubility, and thermal properties of polyvinyl alcohol through natural polymer blending: an approach toward sustainable polymer applications. Polymers (Basel). 2024;16:2141.

24. Yan D, Li Y, Liu Y, Li N, Zhang X, Yan C. Antimicrobial properties of chitosan and chitosan derivatives in the treatment of enteric infections. Molecules. 2021;26:7136.

25. Pramanik S, Aggarwal A, Kadi A, Alhomrani M, Alamri AS, Alsanie WF, Koul K, Deepak A, Bellucci S. Chitosan alchemy: transforming tissue engineering and wound healing. RSC Adv. 2024;14:19219-19256.

26. Türkoğlu GC, Khomarloo N, Mohsenzadeh E, Gospodinova DN, Neznakomova M, Salaün F. PVA-based electrospun materials-a promising route to designing nanofiber mats with desired morphological shape-a review. Int J Mol Sci. 2024;25:1668.

27. Monk JP, Campoli-Richards DM. Ofloxacin. A review of its antibacterial activity, pharmacokinetic properties and therapeutic use. Drugs. 1987;33:346-391.

28. Nash DM, Giles JL. Uterine inflammation and lessons from large animal models of endometritis. Nat Rev Immunol. 2025;25:934-946.

29. Ihrke PJ, Papich MG, DeManuelle TC. The use of fluoroquinolones in veterinary dermatology. Vet Dermatol. 1999;10:193-204.

30. Aramă V. Topical antibiotic therapy in eye infections - myths and certainties in the era of bacterial resistance to antibiotics. Rom J Ophthalmol. 2020;64:245-260.

31. Kumari P, Shukla MK, Tripathi A, Pandey J, Goyal AK. Development of ofloxacin-loaded CS/PVA hydrogel for the treatment of metritis in bovine. Drugs Drug Candidates. 2025;4:17.

32. Yazdanpanah M, Khanmohammadi M, Mehdinavaz Aghdam R, Shabani K, Rajabi M. Optimization of electrospinning process of poly(vinyl alcohol) via response surface methodology (RSM) based on the central composite design. Curr Chem Lett. 2014;3:175-182.

33. Batheja S, Sahoo RK, Rani S, Gupta S, Tejavath KK, Sinha S, Ajazuddin, Yadav AK, Goyal AK, Gupta U. Central composite design based optimization of carbohydrate coated albumin nanoparticles for HCC: synthesis, extensive characterization and in vivo pharmacokinetic evaluation. Biopolymers. 2025;116:e70028.

34. Yang Y, Khan H, Gao S, Khalil AK, Ali N, Khan A, Show PL, Bilal M, Khan H. Fabrication, characterization, and photocatalytic degradation potential of chitosan-conjugated manganese magnetic nano-biocomposite for emerging dye pollutants. Chemosphere. 2022;306:135647.

35. Chaurawal N, Quadir SS, Joshi G, Barkat MA, Alanezi AA, Raza K. Development of fucoidan/polyethyleneimine based sorafenib-loaded self-assembled nanoparticles with machine learning and DoE-ANN implementation: optimization, characterization, and in-vitro assessment for the anticancer drug delivery. Int J Biol Macromol. 2024;279:135123.

36. Hadipour-Goudarzi E, Hemmatinejad N, Shokrgozar MA. Fabrication and DOE optimization of electrospun chitosan/gelatin/PVA nanofibers for skin tissue engineering. Macromol Mater Eng. 2023;308:2200562.

37. Mirzaeei S, Taghe S, Asare-Addo K, Nokhodchi A. Polyvinyl alcohol/chitosan single-layered and polyvinyl alcohol/chitosan/eudragit RL100 multi-layered electrospun nanofibers as an ocular matrix for the controlled release of ofloxacin: an in vitro and in vivo evaluation. AAPS PharmSciTech. 2021;22:170.

38. Daelemans L, Van Paepegem W, D'hooge DR, De Clerck K. Excellent nanofiber adhesion for hybrid polymer materials with high toughness based on matrix interdiffusion during chemical conversion. Adv Funct Mater. 2019;29:1807434

39. Vogt FG, Dell'Orco PC, Diederich AM, Su Q, Wood JL, Zuber GE, Katrincic LM, Mueller RL, Busby DJ, Debrosse CW. A study of variable hydration states in topotecan hydrochloride. J Pharm Biomed Anal. 2006;40:1080-1088.

40. Jinying L, Ying L, Xuan G, Yanli G, Jianping L. Investigation of the release behavior of cupric ion for three types of Cu-IUDs and indomethacin for medicated Cu-IUD in simulated uterine fluid. Contraception. 2008;77:299-302.

41. Uhljar LÉ, Kan SY, Radacsi N, Koutsos V, Szabó-Révész P, Ambrus R. In vitro drug release, permeability, and structural test of ciprofloxacin-loaded nanofibers. Pharmaceutics. 2021;13:556.

42. Ajmal G, Bonde GV, Thokala S, Mittal P, Khan G, Singh J, Pandey VK, Mishra B. Ciprofloxacin HCl and quercetin functionalized electrospun nanofiber membrane: fabrication and its evaluation in full thickness wound healing. Artif Cells Nanomed Biotechnol. 2019;47:228-240.

43. Nair AB, Shah J, Jacob S, Al-Dhubiab BE, Patel V, Sreeharsha N, Shinu P. Development of mucoadhesive buccal film for rizatriptan: in vitro and in vivo evaluation. Pharmaceutics. 2021;13:728.

44. Cruz E, Diniz BV, Ochikubo LM, Kawasaki TE, Veiga FF, Lazarin-Bidóia D, Cesar GB, Radovanovic E, Caetano W, Svidzinski TI, Negri M. Polycaprolactone nanofibers colonized by HeLa cells: an alternative for in vitro investigation of fungal infection. Future Microbiol. 2023;18:199-213.

45. Brighenti MS, Montanheri LRDS, Duque MD, Andreo-Filho N, Lopes PS, Garcia MTJ, Mackenzie L, Leite-Silva VR. In vitro drug release and ex vivo dermal drug permeation studies of selected commercial benzoyl peroxide topical formulations: correlation between human and porcine skin models. Mol Pharm. 2025;22:1365-1372.

46. Dolezel R, Palenik T, Cech S, Kohoutova L, Vyskocil M. Bacterial contamination of the uterus in cows with various clinical types of metritis and endometritis and use of hydrogen peroxide for intrauterine treatment. Vet Med. 2010;55:504-511.

47. Shivhare M, Singh S, Tayeng K, Chakravarti S. Endometrial cytology to diagnose subclinical endometritis in cows. Int J Agric Environ Biotechnol. 2018;11:623-631.

48. Attimarad MV, Nagaraja SH, Setty RS. Simultaneous determination of ofloxacin and flavoxate hydrochloride in human plasma by RP HPLC. J Liq Chromatogr Relat Technol. 2012;35:768-777.

49. Bhoir SI, Gaikwad P, Parab LS, Shringarpure RN, Savant S, Verma PJ. RP-HPLC method development and validation for the simultaneous estimation of satranidazole and ofloxacin in pharmaceutical dosage form. J Chromatogr Sci. 2011;49:84-87.

50. Hughes JH, Upton RN, Reuter SE, Phelps MA, Foster DJR. Optimising time samples for determining area under the curve of pharmacokinetic data using non-compartmental analysis. J Pharm Pharmacol. 2019;71:1635-1644.

51. Romano JE, Thompson JA, Forrest DW, Westhusin ME, Tomaszweski MA, Kraemer DC. Early pregnancy diagnosis by transrectal ultrasonography in dairy cattle. Theriogenology. 2006;66:1034-1041.

52. Rooholghodos SH, Pourmadadi M, Yazdian F, Rashedi H. Optimization of electrospun CQDs-Fe_3O_4-RE loaded PVA-cellulose nanofibrils via central composite design for wound dressing applications: Kinetics and in vitro release study. Int J Biol Macromol. 2023;237:124067.

53. Li D, Xia Y. Electrospinning of nanofibers: reinventing the wheel. Adv Mater. 2004;16:1151-1170.

54. Geng X, Kwon OH, Jang J. Electrospinning of chitosan dissolved in concentrated acetic acid solution. Biomaterials. 2005;26:5427-5432.

55. Huang ZM, Zhang YZ, Kotaki M, Ramakrishna S. A review on polymer nanofibers by electrospinning and their applications in nanocomposites. Compos Sci Technol. 2003;63:2223-2253.

56. Deitzel JM, Kleinmeyer J, Harris D, Beck Tan NC. The effect of processing variables on the morphology of electrospun nanofibers and textiles. Polymer. 2001;42:261-272.

57. Chavanpatil MD, Jain P, Chaudhari S, Shear R, Vavia PR. Novel sustained release, swellable and bioadhesive gastroretentive drug delivery system for ofloxacin. Int J Pharm. 2006;316:86-92.

58. Salama AH, AbouSamra MM, Awad GEA, Mansy SS. Promising bioadhesive ofloxacin-loaded polymeric nanoparticles for the treatment of ocular inflammation: formulation and in vivo evaluation. Drug Deliv Transl Res. 2021;11:1943-1957.

59. Mohite P, Puri A, Munde S, Dave R, Khan S, Patil R, Singh AK, Tipduangta P, Singh S, Chittasupho C. Potential of chitosan/gelatin-based nanofibers in delivering drugs for the management of varied complications: a review. Polymers (Basel). 2025;17:435.

60. Chinnappan BA, Krishnaswamy M, Xu H, Hoque ME. Electrospinning of biomedical nanofibers/nanomembranes: effects of process parameters. Polymers (Basel). 2022;14:3719.

61. Liang X, Zhong HJ, Ding H, Yu B, Ma X, Liu X, Chong CM, He J. Polyvinyl alcohol (PVA)-based hydrogels: recent progress in fabrication, properties, and multifunctional applications. Polymers (Basel). 2024;16:2755.

62. Garnica-Palafox IM, Sánchez-Arévalo FM. Influence of natural and synthetic crosslinking reagents on the structural and mechanical properties of chitosan-based hybrid hydrogels. Carbohydr Polym. 2016;151:1073-1081.

63. Ahmad Wsoo M, Izwan Abd Razak S, Shahir S, Ahmed Abdullah Al-Moalemi H, Rafiq Abdul Kadir M, Hasraf Mat Nayan N. Development of prolonged drug delivery system using electrospun cellulose acetate/polycaprolactone nanofibers: future subcutaneous implantation. Polym Adv Technol. 2021;32:3664-3678.

64. Vashisth P, Raghuwanshi N, Srivastava AK, Singh H, Nagar H, Pruthi V. Ofloxacin loaded gellan/PVA nanofibers - synthesis, characterization and evaluation of their gastroretentive/mucoadhesive drug delivery potential. Mater Sci Eng C Mater Biol Appl. 2017;71:611-619.

65. Mosallanezhad P, Rajabifar N, Rostami A, Ahmadi Z, Taghdimi R, Nazockdast H. Preparation and structural analyses of antimicrobial core-shell chitosan-polycaprolactone nanofibers for controlled curcumin release. Colloids Surfaces A Physicochem Eng Asp. 2025;716:136736.

66. Brako F, Thorogate R, Mahalingam S, Raimi-Abraham B, Craig DQM, Edirisinghe M. Mucoadhesion of progesterone-loaded drug delivery nanofiber constructs. ACS Appl Mater Interfaces. 2018;10:13381-13389.

67. Gavali P, Desai J, Shah P, Sawarkar S. Transmucosal delivery of peptides and proteins through nanofibers: current status and emerging developments. AAPS PharmSciTech. 2024;25:74.

68. Sola P, Garikapati KK, Krishnamurthy PT, Kumari M. Polysorbate 80 surface modified SLNs of formoterol suppress SNCA gene and mitochondrial oxidative stress in mice model of Parkinson's disease. Sci Rep. 2023;13:19942.

69. Becerra SC, Roy DC, Sanchez CJ, Christy RJ, Burmeister DM. An optimized staining technique for the detection of Gram positive and gram negative bacteria within tissue. BMC Res Notes. 2016;9:216.

70. Gonzalez Moreno C, Torres Luque A, Oliszewski R, Rosa RJ, Otero MC. Characterization of native *Escherichia coli* populations from bovine vagina of healthy heifers and cows with postpartum uterine disease. PLoS One. 2020;15:e0228294.

71. Plöntzke J, Madoz LV, De la Sota RL, Drillich M, Heuwieser W. Subclinical endometritis and its impact on reproductive performance in grazing dairy cattle in Argentina. Anim Reprod Sci. 2010;122:52-57.

72. Damarany AI. Physical traits of vaginal mucus discharge and their relations to conception rate of Egyptain Baladi cows. Egypt J Anim Prod. 2020;57:63-70.

73. Hässig M, Steinmann B, Wittenbrink MM. Nutzen von klinischen und labordiagnostischen Parametern zur Diagnostik der Endometritis beim Rind [Benefit of clinical and laboratory parameters for the diagnosis of endometritis in dairy cows]. Schweiz Arch Tierheilkd. 2010;152:411-416.

74. Bartolome ND, Jongsuwanwattana R, Asawakarn S, Suadsong S, Sangpradit K, Swangchan-Uthai T. Assessment of the physical and chemical properties of vaginal discharge for the diagnosis of endometritis in dairy cattle. 2025;18:1322-1332.

75. Cui Z, Zheng Z, Lin L, Si J, Wang Q, Peng X, Chen W. Electrospinning and crosslinking of polyvinyl alcohol/chitosan composite nanofiber for transdermal drug delivery. Adv Polym Technol. 2018;37:1917-1928.

76. Qureshi D, Pattanaik S, Mohanty B, Anis A, Kulikouskaya V, Hileuskaya K, Agabekov V, Sarkar P, Maji S, Pal K. Preparation of novel poly (vinyl alcohol)/chitosan lactate-based phase-separated composite films for UV-shielding and drug delivery applications. Polym Bull. 2022;79:3253-3290.